

5-2017

Electrical Optimization of a Plug-In Hybrid Electric Vehicle

Andre J. Napier

Follow this and additional works at: <https://commons.erau.edu/edt>



Part of the [Automotive Engineering Commons](#), and the [Electrical and Computer Engineering Commons](#)

Scholarly Commons Citation

Napier, Andre J., "Electrical Optimization of a Plug-In Hybrid Electric Vehicle" (2017). *Dissertations and Theses*. 342.

<https://commons.erau.edu/edt/342>

This Thesis - Open Access is brought to you for free and open access by Scholarly Commons. It has been accepted for inclusion in Dissertations and Theses by an authorized administrator of Scholarly Commons. For more information, please contact commons@erau.edu.

ELECTRICAL OPTIMIZATION OF A PLUG-IN HYBRID ELECTRIC VEHICLE

By

Andre J. Napier

A Thesis Submitted to the College of Engineering Department of Electrical
Engineering in Partial Fulfillment of the Requirements for the Degree of
Master of Science in Electrical and Computer Engineering

May 2017

Embry Riddle Aeronautical University
Daytona Beach, Florida

ELECTRICAL OPTIMIZATION OF A PLUG-IN HYBRID ELECTRIC VEHICLE

by

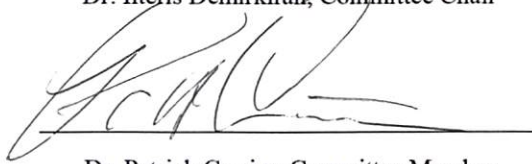
Andre J. Napier

This thesis was prepared under the direction of the candidate's thesis committee Chair Dr. Ilteris Demirkiran, Department of Electrical, Computer, Software & Systems Engineering, and has been approved by the members of the thesis committee. It was submitted to the Department of Electrical, Computer, Software & Systems Engineering and was accepted in partial fulfillment of the requirements for the degree of Master of Science in Electrical and Computer Engineering.


THESIS COMMITTEE



Dr. Ilteris Demirkiran, Committee Chair



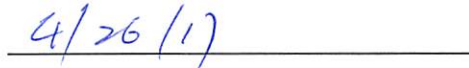
Dr. Patrick Currier, Committee Member



Dr. Tianyu Yang, Committee Member,



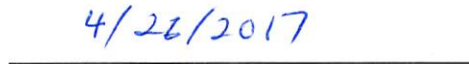
Dr. Timothy A Wilson, Department Chair
or Dr. Jianhua Liu, Graduate Program Chair



Date




Dr. Maj Mirmirani, Dean of College of Engineering



Date



Dr. Christopher D. Grant, Vice Chancellor for
Academics



Date

Abstract

Hybrid electric vehicles electrification and optimization is a prominent part of today's automotive industry. GM and the Department of Energy challenge 16 universities across North America to redesign a Chevrolet Camaro into a hybrid electric vehicle. This thesis will address how Embry Riddle Aeronautical University's EcoCAR team electrified and optimized the vehicle. The objective of the thesis is to optimize the electric portion of the vehicle, particularly the low voltage circuitry. Prior work is discussed in detail on the vehicle communication bus, building the power distribution unit and the approach the electrical team took when building the electric portion of the vehicle. Simulations were done based on manufacturer data and bench tests to create an ideal model. Data was collected from the vehicle and compared to the ideal model to determine errors in the electrical system. An emphasis was placed on critical and high power components to simplify the simulation model. The issues found were alleviated by conducting research, using research analysis, physically changing the system or by implementing control strategies. Most of the issues came from the power distribution unit, and implementation techniques such as grounding. The MOSFETs within the power distribution unit was not fully turning on and off, and which was due to a slow RC time constant occurring on the gate of the transistors. By replacing the resistors, this issue was mitigated. Every problem found was properly mitigated to an acceptable industry or research standard.

Acknowledgements

First and foremost, I would like to express my gratitude to my thesis advisor Dr. Ilteris Demirkiran for his guidance and support throughout the years. His continued support has helped me accomplish many goals both in research and academically. This work would not be possible without the support of the electrical, computer, software, & systems and mechanical engineering departments that provided me with the material and equipment required to record data and perform analysis. I want to give a special thanks to my project advisor Dr. Patrick Currier and Dr. Thomas Yang. Also, my sincere thanks to Mr. Michael Potash and Dr. Jianhua Liu for their help with several of my circuit designs and conversation on the vehicle's circuit problems. I also want to thank my fellow teammate Matthew Gileau for his help in attaining data for the research conducted and determining technical issues. I want to give another special thanks to Matthew Nelson for his support on logging data and cooperation with adjusting his control strategies to improve the electrical systems.

Finally, I want to thank my parents for their prayers and continued support of my educational decisions and goals. To my fiancé, Felicia Hall, for continuously keeping me focused on the mundane, yet blissful world.

This thesis is dedicated to the undeserved communities of The Bahamas and The United States.

Table of Contents

Contents

Abstract.....	ii
Acknowledgements.....	ii
Table of Contents.....	iv
Table of Figures	vii
List of Tables	x
Chapter 1. Introduction	1
1.1 Background.....	3
1.1.1 CAN Bus.....	4
1.1.2 What is CAN Bus?.....	5
1.1.3 Purpose of Research.....	6
1.1.4 Six Inch CAN Bus	7
1.1.5 Relay	8
1.1.6 CAN Bus Dynamics.....	8
1.1.7 Testing Against EMI.....	9
1.1.8 CAN Bus Conclusion.....	10
1.1.9 Power Distribution Unit.....	10
1.1.10 Electrical Design.....	10
1.1.11 Physical Design.....	12
1.1.12 Thermal Design.....	13
1.1.13 Vehicle Work.....	14
1.1.14 System Engineering	15
1.1.15 Architecture Design	19
1.1.16 Electrical Implementation	21
1.1.17 Integration	25
1.1.18 Testing.....	26
1.1.19 Verification	26
Chapter 2 Literature Review	28
2.1 Power System Issues.....	28
2.2 Noisy Automotive Environments.....	31
2.3 Ground Noise	32

2.4 Measurement.....	33
2.5 Simulating a Lead-Acid Battery	34
2.6 Simulating Loads	35
2.7 Lead Acid Battery Charging	36
2.8 Voltage Ripple and DC/DC converters.....	36
Chapter 3. HV Optimization	38
3.1 Operation and Analysis of the Inverter	38
3.2 Inverter Electrical and Thermal Module	42
3.3 DC/DC converter Electrical and Thermal Module	42
3.4 Asynchronous 3-phase Electric Motors	43
3.5 Inverter data Analysis	43
3.6 DC/DC Data Analysis.....	44
3.7 Overall System Analysis.....	45
3.10 HV Conclusion.....	47
Chapter 4. LV Optimization	48
4.1 LV Ideal Simulation.....	49
4.2 LV Vehicle Measurements	52
4.3 LV Comparison & Analysis.....	53
4.4 LV Mitigation	53
4.5 Aux Battery.....	54
4.5.1 Aux Battery Simulations.....	55
4.5.2 Aux Battery Vehicle Measurements	55
4.5.3 Aux Battery Simulations & Comparison	58
4.5.4 Aux Battery Mitigations	61
4.6 DC/DC Converter	63
4.6.1 DC-DC Converter Simulations	63
4.6.2 DC-DC Converter Vehicle Measurements	64
4.6.3 DC-DC Converter Simulations & Comparison.....	66
4.6.4 DC-DC Converter Mitigations.....	67
4.7 Power Distribution Unit.....	67
4.7.1 Power Distribution Unit Simulations	68
4.7.2 Power Distribution Unit Measurements.....	69
4.7.4 Power Distribution Unit Mitigations.....	71

4.8	Supervisory Controller.....	72
4.8.1	Supervisory Controller Simulations.....	72
4.8.2	Supervisory Controller Measurements.....	73
4.8.3	Supervisory Controller Simulations & Comparison	74
4.8.4	Supervisory Controller Mitigations	76
4.9	Voltage Ripple	76
4.9.2	Voltage Ripple Measurements	76
4.9.4	Voltage Ripple Mitigations	78
4.10	Additional Analysis	79
4.10.1	EMI & HVIL Measurements	79
4.10.2	EMI & HVIL Research	81
4.10.3	EMI & HVIL Mitigations	80
4.10.5	Parasitic Draw.....	81
4.10.4	LV Conclusion.....	81
Chapter 5.	Conclusion.....	83
5.1	Conclusion	83
5.2	Future Work.....	84
Chapter 6	References	85
Chapter 7	Appendix	87
7.1	Appendix A.....	87
7.1	Appendix B.....	88
7.1	Appendix C	90
7.1	Appendix D.....	91
7.1	Appendix E	94

Table of Figures

Figure 1: Vehicle Architecture.....	2
Figure 2: Electrical Architecture.....	3
Figure 3: EcoCar 2 Vehicle, Chevy Malibu.....	5
Figure 4: CAN Bus Topology.....	6
Figure 5: Initial Vehicle CAN bus design.....	7
Figure 6: Modified Vehicle CAN bus design	7
Figure 7: 6 inch CAN bus	7
Figure 8: Power Distribution Unit Low Current Circuit.....	11
Figure 9: Power Distribution Unit Low Current Printed Circuit Board.....	11
Figure 10: High Current Circuit Print Circuit Board	12
Figure 11: Power Distribution Enclosure.....	13
Figure 12: HV Sub System Components	20
Figure 13: LV Sub System Components.....	20
Figure 14: CAN Bus Sub System Bus Connections	21
Figure 15: ESS Implementation plan	23
Figure 16: LV ESS Implementation plan.....	24
Figure 17: LV Engine Implementation Plan	25
Figure 18: CAN bus Implementation Plan.....	25
Figure 19: Supply Line Transients.....	29
Figure 20: Basic Ground Loop	33
Figure 21: Linear Electrical Model.....	35
Figure 22: Physical Structure of Module	40
Figure 23: Thermal RC network	41
Figure 24: Thermal Model.....	42
Figure 25: DC-DC Converter Model	43
Figure 26: Inverter Current	44
Figure 27: Junction Temperature Output of IGBT's	44
Figure 28: DC/DC Voltage output - 14.3V.....	45
Figure 29: DC/DC Current Output	45
Figure 30: Overall Model.....	46
Figure 31: IGBT Power Losses.....	46
Figure 32: Overall Model.....	50
Figure 33: Accessory Load Model.....	50
Figure 34: Engine Loads	51
Figure 35: Lead Acid Battery Model	55
Figure 36: Battery Initial Startup Voltage.....	56
Figure 37: Battery Initial Startup Current	57
Figure 38: Battery Voltage (Parked) Engine On.....	57
Figure 39: Battery Current (Parked) Engine On	58
Figure 40: Battery Voltage with no accessory of Run/Crank	59
Figure 41: Battery Current with no accessory or Run/Crank.....	60

Figure 42: Battery Current (Parked) Engine On	60
Figure 43: Battery Voltage (Parked) Engine on Comparison	61
Figure 44: Battery over Current Charge Deplete Mode	62
Figure 45: DC-DC Model.....	64
Figure 46: DC/DC Voltage (Parked) Engine On	64
Figure 47: DC/DC Current (Parked) Engine On.....	65
Figure 48: DC/DC Converter Initial Startup Voltage	66
Figure 49: DC-DC Voltage (Parked) Engine On	66
Figure 50: DC-DC Current (Parked) On)	67
Figure 51: HV Electrical Cooling Pump Model	69
Figure 52: Electric motors water pump source voltage	69
Figure 53: Zoom into power distribution module initial voltage	70
Figure 54: Gate of radiator fan MOSFET	70
Figure 55: Mbed PWM signal output	71
Figure 56: MOSFET Gate Voltage after Mitigation.....	72
Figure 57: MicroAutoBox Model	73
Figure 58: MicroAuto Box Initial Startup Voltage.....	73
Figure 59: Voltage sag from Figure 59.....	74
Figure 60: MicroAuto Box Initial Startup Current	74
Figure 61: Supervisory Controller, simulation and empirical data Compared	75
Figure 62: MabX Current simulated and measured overlap	75
Figure 63: Voltage Ripple on 12v system before mitigation	77
Figure 64: Requested Throttle vs Actual throttle	77
Figure 65: Ripple voltage and Current.....	78
Figure 66: Mitigated Requested Pedal vs Actual Pedal	79
Figure 67: EMI Reading Across the DC Lines	80
Figure 68: DC Lines into the Inverter.....	80
Figure 69: EMI Reading on Three Phase Cables to Motors	81
Figure 70: HVIL Voltage Drop.....	81
Figure 71: High Level Schematic for HVIL Circuit.....	81
Figure 72: VDS of implemented P-channel MOSET	81
Figure 73: Schematic for new HVIL circuit	81
Figure 74: 12v Battery sleep mode Current.....	81
Figure 75: 12v Battery full sleep mode current draw	81
A 1: HV Inverter with Motor Model.....	87
A 2: Overall added components model.....	87
B 1: Stock Key in Current.....	88
B 2: Stock Key out Current (amps).....	88
B 3: Stock Accessory Loads Current (amps)	89
B 4: Stock Crank Current (Amps)	89
B 5: Stock Engine Idle Current (Amps) Data	90
D 1: More Battery Charging Current	91
D 2: DC-DC Transient/Initial Turn on.....	92
D 3: More Supervisory Current Draw Data with engine on	92

D 4: Too many ground at one post.....	93
D 5: Grounds removed.....	93
D 6: Verified Parasitic Current Draw from 12v battery.....	93
E 1: Hall Effect Current Sensor used for measuring currents greater than 2 amps.....	94
E 2: Lead Acid Battery Discharge Standards and Calculations.....	95

List of Tables

Table 1: Measurement Equipment Used..... 53

Table 2: RLC Simulation Values 91

Chapter 1. Introduction

Vehicles that utilize batteries which can be recharged using a power grid are classified as Plug-in Hybrid Electric Vehicles (PHEVs). They consist of motors, inverters, DC-DC converters and an internal combustion engine (ICE). Within the vehicle, drivers have the choice of operating only the ICE, the battery power, or both simultaneously.

EcoCAR 3 is a four-year competition sponsored by the Department of Energy and General Motors. Sixteen universities across North America are challenged with the task of redesigning a gasoline powered Chevrolet Camaro into a plug-in hybrid electric vehicle. Students must implement their designs while still maintaining the “muscle” and performance expected from the iconic car [1].

The Embry Riddle Aeronautical University EcoCAR 3 team developed a parallel two-clutch system (P2-P2) PHEV that can operate in both series and parallel hybrid configurations with 100% rear wheel torque. A 350v, 18.9KWh lithium ion battery pack, two electric motors, which are controlled by the inverters, and a 2.4L GM LEA ECOTec engine are used to provide the required torque to the wheels. The vehicle’s architecture is shown in Figure 1.

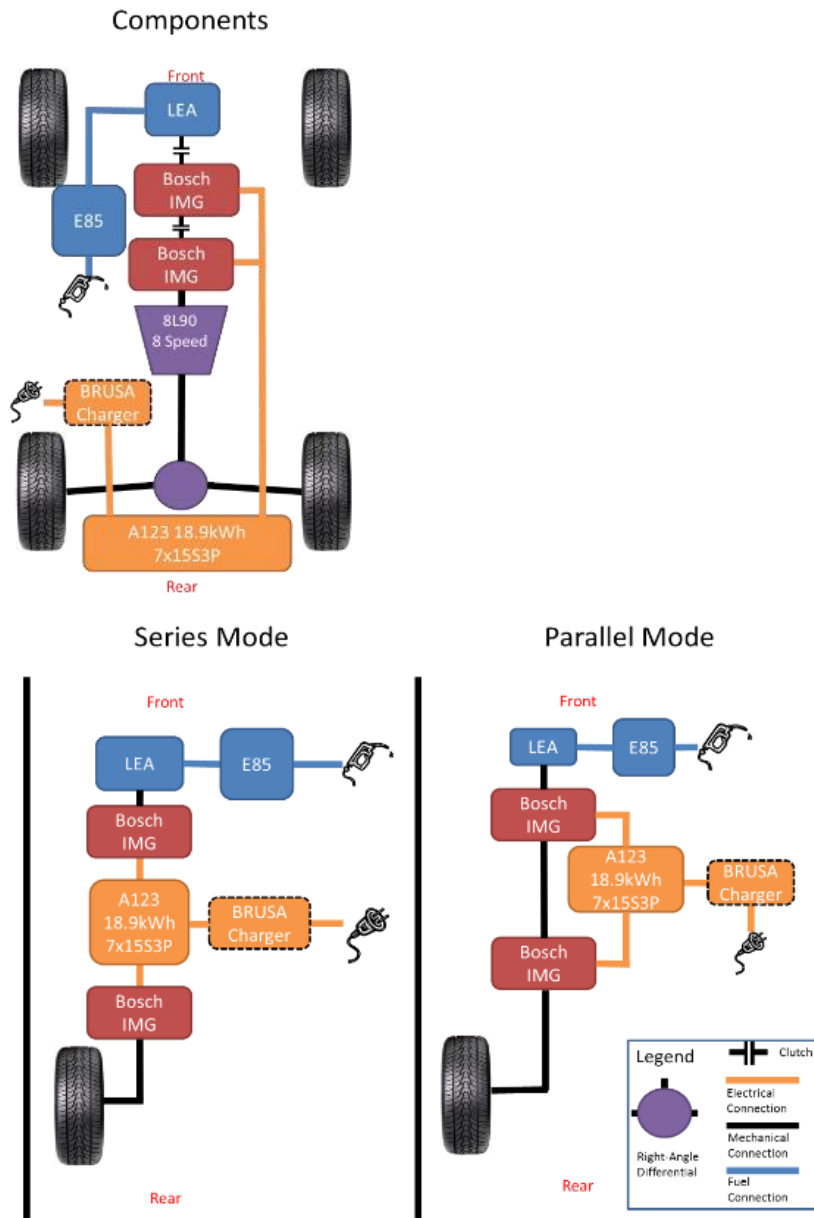


Figure 1: Vehicle Architecture

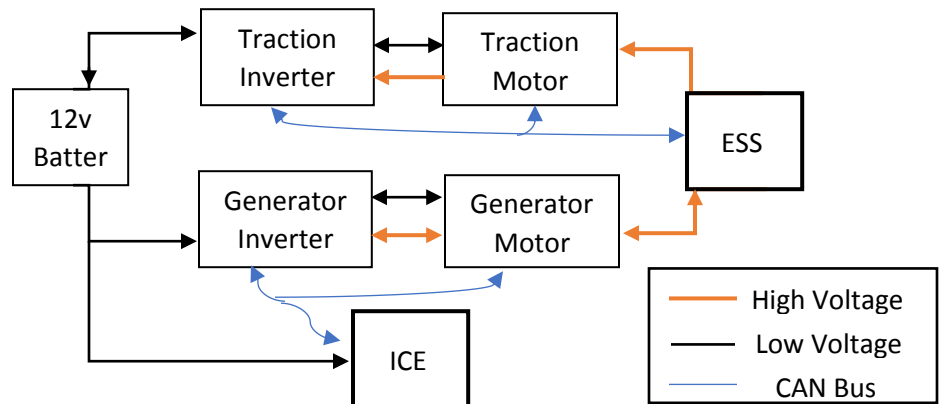


Figure 2: Electrical Architecture

The architecture (Figure 1) is a high-level overview of the vehicle system. The electrical systems are displayed with more detail in Figure 2; the HV sub-system and low voltage sub-system are portrayed more distinctly. The HV components include the Brusa charger, the Energy storage system (ESS), an A/C compressor, two power electronic module (PEM), which consists of a 3-phase inverter and a DC/DC converter, and two 3-phase motors.

The low voltage sub-system entails a larger number of components consisting of all high voltage components, along with a power distribution module, the LEA engine electrical harness, fuel driver, a proximity box, high voltage interlock system (HVIL), CAN busses, and a supervisory controller.

In this study, the electrical system's critical components are analyzed to determine the electrical standing of the system. Upon conducting this study, the electrical system is 95% complete. Every critical component is integrated, and tested for over 400 miles. The system underwent both high speed and low speed testing without any issues occurring during operation. By testing the electrical system to this extent, the system was validated based on team requirements. This thesis will verify the electrical system is built right and addresses the portions that are not.

The verification process began with simulations based on the manufacture's data and isolated bench tests. Vehicle measurements are then taken post processed and compared to the ideal simulation data. Data deviating more than 20% outside the ideal simulation or bench test data were addressed, or a plan is given for the control team to mitigate problems. Research and circuit analysis was done to theoretically solve each problem and physical implementation was done to mitigate the issue.

1.1 Background

The success of this project was due to previous research and preventative work that was done over the course of three years. With the experience of advisors, previous team members and current team

members, much of the preventative work was done due to previous experiences, both successful and failures.

Year one of EcoCAR 3 was used to conduct research for future work and determining the vehicle's architecture. Based on problems that occur within EcoCAR 2 competition research was done to prevent previous problems from occurring. There were three main problems encountered during EcoCAR 2 competition, namely, solder joint problems throughout the vehicle, CAN bus issues and a power distribution issue. Year one of EcoCAR 3 was used to determine ways of overcoming these problems that may occur in the future.

1.1.1 CAN Bus

Throughout working with the EcoCAR program, there arose several problems. The vehicle's relay box was unable to actuate systems properly and Supervisory Control Unit had issues communicating over the Control Area Network (CAN). The traction motor could not spin the wheels of the vehicle, because of the inverter. The Brusa was unable to charge the energy storage system. A diagram is shown below on the vehicle's electrical components. The relay box issue was corrected by thoroughly going through the vehicle's wire harness. The traction motors, the inverters, and the Brusa were all high voltage related problems, but they all utilized the CAN bus. There were problems with the wire harness and the Control Area Network (CAN) bus within the vehicle. These problems brought forth many issues within EcoCAR 2 year 3. One of which occurred when the vehicle reached high speeds. The vehicle shuttered and related error messages to the vehicle's main microcontroller. After an analysis was done on the CAN bus it was assumed that there was an impedance mismatch due to the length of stubs and the bus itself. To understand the problem further investigation and research was required.

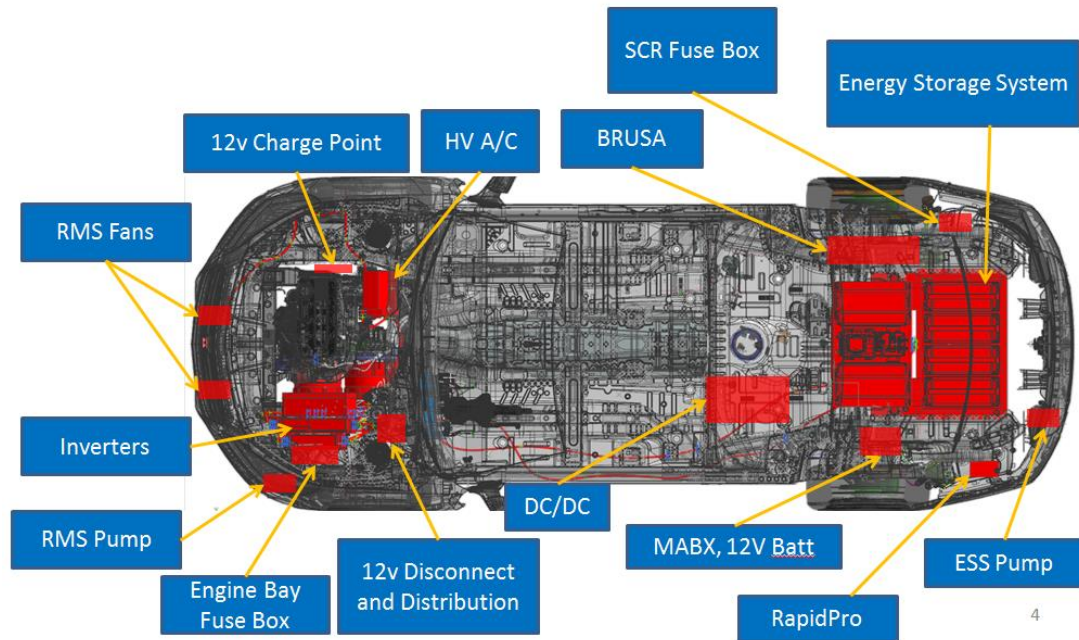


Figure 3: EcoCar 2 Vehicle, Chevy Malibu

1.1.2 What is CAN Bus?

CAN bus is a serial communication system that uses a two wire topology to communicate between 8-16 bit microcontrollers. The protocol was created by the engineering company Robert Bosch GmbH in the mid 1980's, to be used in vehicles. During the early 1990's it was made a standard by the International Organization for Standardization. There is low and high speed CAN communication, where high speed CAN communication is done at 40Kbits/sec -1Mbits/s, and the wires are terminated with 120 at both ends of the bus and low speed CAN utilizes 40Kbits/sec-125Kbit/sec with terminations at each device.

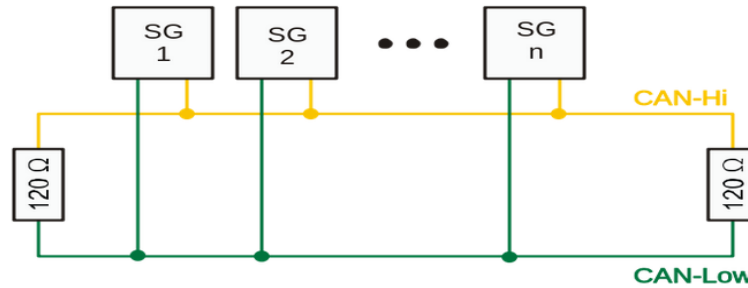


Figure 4: CAN Bus Topology

1.1.3 Purpose of Research

The purpose of this research effort is to address the problems mentioned early in the manuscript, and to understand the limitations of the CAN bus systems and its limiting factors for future implementation. For testing purposes, it was required to create an operable CAN bus to control a relay using a microcontroller, and a Vector CANcase. The goal of this research effort is to bring forth a better understanding of a CAN bus, and to determine universal limiting factors and efficiency.

Issues with the CAN bus were widespread, and how to solve the problem was uncertain. Research was done to build a CAN bus test bench system to simplify testing. This made it easier to build a robust and reliable system outside of the vehicle. The findings from the experiment were compared to the malfunctioning set up within the vehicle. Based on the finding it was determined that the problem was in the length of the CAN bus stubs. Further research was carried out on the CAN bus system to implement more reliable communication schemes and to avoid problems.

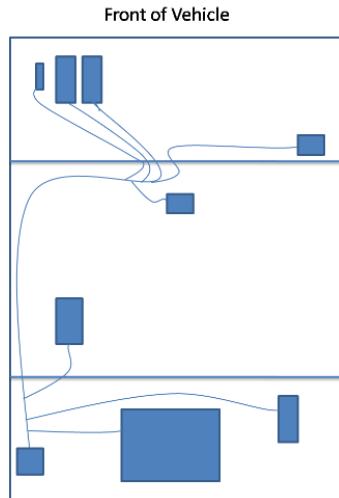


Figure 5: Initial Vehicle CAN bus design

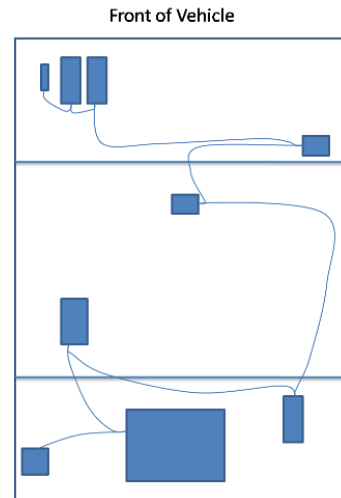


Figure 6: Modified Vehicle CAN bus design

The first task was to create a CAN bus system and control that network using a relay and determine its functionalities. More CAN bus systems were created with different lengths, characteristics, such as insulation shielding, wire shielding or drain and factory twisted pair cables versus non-twisted pair cables.

1.1.4 Six Inch CAN Bus

Initially, several CAN bus systems were created to simplify run test. The first CAN bus was created 6 inches in length, not shielded, with a CAN drain connected, which was a non-twisted pair of cables. Each connection was soldered to a DB-9 connector with no further nodes nor stubs in between. A basic communication code was created to transmit messages across the bus using an Arduino. The messages sent were basic numbers from 0-7, 8 numbers in total. A vector CAN case was used as the receiving device and also to view the messages being sent across the bus. A layout of the connection is shown below in Figure 7.

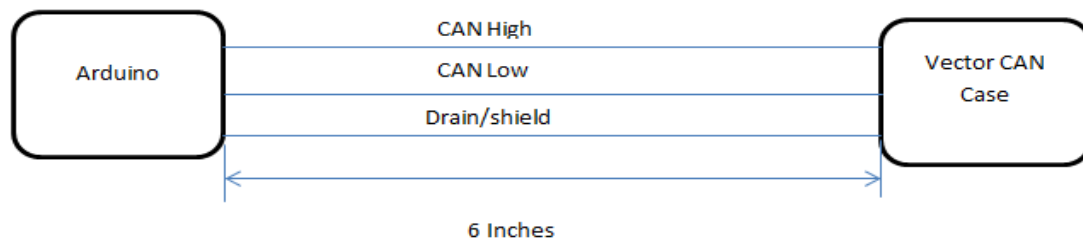


Figure 7: 6 inch CAN bus

1.1.5 Relay

The relay controlled CAN bus was controlled using another Arduino board. Supply power came from a 12V d/c source to the relay which was controlled by a transistor whose base was connected to the second Arduino's digital output. With this setup, a CAN bus can be controlled using a relay under certain conditions. One of the reasons could be due to time/periodicity or relevance. The information being processed might be periodic over a considerable time frame which may draw unnecessary power or cause a strain on the primary CAN bus. Another relay controlled CAN bus was designed using 1 Arduino board in which the relay's coil was controlled by a digital pin using a transistor. The CAN high bus being connected to the normally closed lead relays.

1.1.6 CAN Bus Dynamics

After creating a relay controlled CAN Bus, the relay was removed and the dynamics of the CAN bus was tested. It was determined by testing that the CAN bus operated in two distinct states, namely recessive and dominant, recessive being the state of zero differential voltage and the dominant being the state with a differential voltage of 2V. In the dominant state the current flowing through the high bus fluctuated at $30\text{mA} \pm 1\text{mA}$ with 3.5V phase to ground. The low bus had a current and a voltage of $12\text{mA} \pm 0.5\text{mA}$ and 1.5V respectively. Whereas in the recessive state the current and voltage was measured to be approximately $20\text{mA} \pm 1\text{mA}$ and 2.5V respectively on both busses. These measurements yield

$$R = \frac{V}{I} = \frac{3.5V}{0.03A} = \frac{1.5V}{0.012A} = \frac{2.5V}{0.02A} = 120\Omega$$

(1)

This result agrees with the 120 resistor terminations at the end of each bus.

Nonetheless, these measurements changed under certain conditions. When a variable resistor was placed on the bus centered between the 120 resistors the voltage dropped on the bus and so did the current. The system self-maintained a voltage difference of roughly 1.5 V continuously until the high impedance dropped the CAN-high bus voltage below 1.5V, which caused a differential of less

than 1.5V between the 2 busses. Distortion of the signal occurred when the CAN-high bus dropped to 1.8V and became inoperable at about 0.8V.

1.1.7 Testing Against EMI

The primary limitation tested was the electromagnetic interference (EMI) immunity of the CAN bus system. Initially, the 6 inch, unshielded, CAN bus from Figure 7 was tested by placing it less than an inch away from a circuit distributing roughly 37 watts of power, the voltage being 12V direct current (d/c), and the current being 3A. This experiment produced no error messages on the vector Canoe message trace window; each message was fully transmitted. With no distortion, another test was conducted to create greater EMI. A solenoid was constructed around the CAN bus with a length of roughly 3.5 inches and a half inch diameter. The solenoid is roughly 0.5833% of the CAN bus length. When allowing 3A to flow throughout the solenoid the CAN signal appeared undisturbed. To increase the EMI from the solenoid, a relay was used to control the current flowing through it. The relay was opened and closed manually and with this method the signals were still not distorted. Using an EMI/ghost meter the solenoid produced an electromagnetic field (EMF) radiation between 2~30m Gauss. Transformers were then used to create larger EMI from the solenoid by opening and closing a switch manually. The EMF rose to over 100m Gauss, but the CAN bus was still unaffected. These tests were also performed on 3 feet and 7 feet, shielded and twisted paired CAN buses and there weren't any signs of distortion.

Unable to determine the CAN bus distortion environment, the drain wire was removed to reduce immunity and test the drain's integrity. Using the relay and manually toggling the switch, the CAN signal distorted at approximately 9.3mG. Increasing the EMF to over 100mG could not completely distort the signals; nonetheless, the drain's integrity was tested. A CAN bus 3 feet long, twisted paired, with shielding and no drain connected was then placed in a solenoid with a length of 21 inches. This length being 0.5833% of the 3 feet CAN bus length. With this solenoid, the CAN bus

was distorted at 5.7m Gauss. Again, this CAN Bus could not be completely distorted with EMIs over 100m Gauss.

1.1.8 CAN Bus Conclusion

Based on the results, CAN networks appear to lose robustness based on length, the impedance of the line, and the wire drain, with the drain not being a required feature, but a beneficial factor. The excess stub lengths of the CAN bus within the vehicle increased the lines impedance and thus increased the line's reflections. After reimplementation, the new stub lengths was less than 3 inches. Thus, the CAN bus produced errors when the vehicle produced higher EMF. The results show that the drain itself increases the EMF immunity by more than a factor of ten.

1.1.9 Power Distribution Unit

A power distribution box was created to control the high current devices throughout vehicle. The box itself was designed from the ground up. The box was designed to communicate over control area network and distribute up to 30 amps of current from a nominally 12v voltage source. Due to packaging restraints, the unit was designed as small as possible based on the size of the connectors. Thermal restraints were also accounted for within the design because the unit would be placed within the engine bay.

1.1.10 Electrical Design

The microcontroller used to control the unit's internal components is a mBed LPC1768. The microcontroller was chosen simply because of its price and ability to easily be integrated with a CAN transceiver. To reduce the amount current flowing throughout this system MOSFETs were used. Because the power distribution unit was determined to be a high side driver, the high current transistors chosen were P-channel MOSFETs.

The unit was broken up into high and low current circuits. The low current circuit is given in Figure 8. The low current circuit consists of two voltage regulators. The first regulator is a 12v regulator

The schematic illustrates a complex electronic system, likely a multi-channel analyzer or a precision measurement device. Key components include:

- Input Stages:** Multiple channels of input signals are processed by TL072 operational amplifiers configured as buffers or comparators. These are connected to a PIC16F877A microcontroller.
- Microcontroller:** A PIC16F877A is the central processing unit, managing the logic and timing of the system. Its pins are extensively connected to other components.
- Output Drivers:** TDA1050 integrated circuits serve as output drivers, converting digital signals from the microcontroller into analog outputs.
- Power Management:** The circuit includes voltage regulators (e.g., 7805, 78L05) and decoupling capacitors to ensure stable power supply across different operating voltages (5V, 12V).
- Timing and Signal Conditioning:** Various resistors and capacitors are used for timing networks, signal conditioning, and impedance matching throughout the circuit.

11

A separate board was used for the high current circuit to keep the enclosure as small as possible. The high current circuit consists of four MOSFETs with protection diodes for back electromagnetic force caused by the inductive circuits. Each MOSFET was chosen to carry 30 amps. The traces of the printed circuit board were calculated using advanced circuit trace calculator. See the PCB boards in Figure 10.

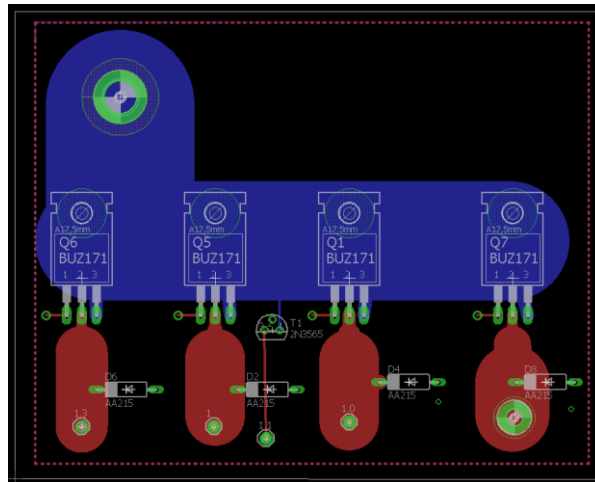


Figure 10: High Current Circuit Print Circuit Board

1.1.11 Physical Design

After configuring and designing all the new vehicle components in CAD, the vehicle has limited space for components larger than 5 inches by 3 inches by 4 inches. Based on the electrical limitations, the PCB would be capable of fitting inside of an enclosure that meets the specs. The biggest limitation then is the connectors necessary to interface between the PCB and the vehicle.

The enclosure has an eight-gauge wire to power the high current circuit PCB with another four twelve gauge wires leaving the board to the vehicles components. The low current circuit has a

power supply and ground wire entering the unit with four sensor wires and two CAN wires leaving the box. The four trigger leads connect from the high current board to the low current board with the enclosure itself.

Figure 11 shows the enclosure with the connectors modeled in CAD. The model was created simply to model the enclosure with the PCB and the connectors to verify that the design would work before purchasing. Heat sinks were not necessary to be considered within the design, so thus did not get modeled into the CAD design. In designing the enclosure, the automotive environment was considered. The enclosure was designed to be splash proof (IP 65) rated and capable of withstanding engine temperatures without deformation.

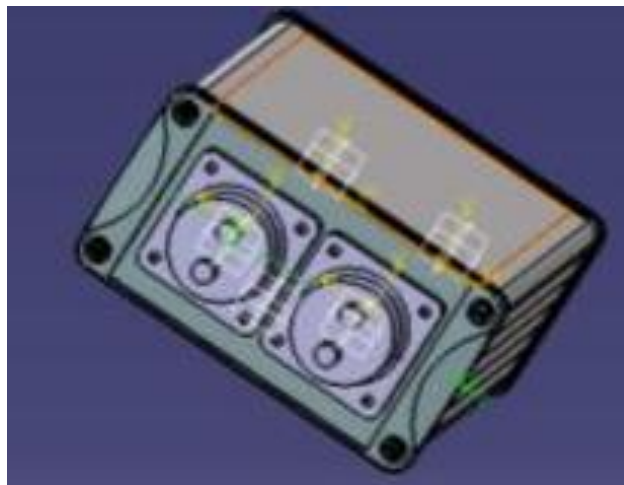


Figure 11: Power Distribution Enclosure

1.1.12 Thermal Design

Thermal considerations were greatly considered within this design. The MOSFETs were chosen to have a turn on resistance of at least $10\text{ m}\Omega$. With this size turn on resistance there was no need to add a heat sink. To prove that there was no heat sink needed, a basic calculation was done, see equation 1. The MOSFET's 'on' resistance is $6\text{ m}\Omega$ with a maximum operating power rating of two watts. Each load draws ten amps continuously. A twenty percent margin was incorporated into the calculation to account for erroneous error and longevity.

$$\text{Power (P)} = I^2 R$$

(2)

$$\text{Current (I)} = 10 \text{ amps}$$

$$\text{Resistance (R)} = 6\text{m}\Omega$$

$$= 12^2 * 0.0065$$

$$= 0.936 \text{ watts}$$

Based on the given calculation additional heat protection is not necessary. The power rating used however is assuming an ambient temperature of 25° C. If the ambient temperature increases above 25° C, the power rating decreases linearly from two watts to zero watts. The engine bay is expected to reach temperatures of 70- 95 degrees Celsius. Using this ambient temperature, the maximum power rating of the MOSFET is then one watt on the extreme end. Based on the new assumptions the MOSFET can still operate effectively, however a small heat sink was added to each MOSFET to ensure continuous operation.

After testing the unit got hotter than expected since the box was placed near the exhaust, which can easily reach temperatures up to 400 degrees Celsius. While the vehicle was driving, the unit could operate, but at idle or while charging the ESS with the engine as the vehicle stood stationary the unit overheated, causing the microcontroller to shut down and causing the MOSFET to overheat. Because of this, the unit was removed away from the exhaust by six inches. At this distance, the power distribution unit could operate and remain under 85 degrees Celsius.

1.1.13 Vehicle Work

The electrical team was tasked with implementing a fully electric Chevrolet Camaro in three months with full functionality. In order to meet deadlines with minimal errors, a great deal of planning and collaboration was done with regards to every component. Project management was

required in order to ensure proper training and goals were being met. Later the paper will discuss the methods used.

Safety was a high priority when it came to vehicle design. The electrical design included features like high voltage inter-lock system (HVIL), emergency stop buttons, and a 12V disconnect switch. The HVIL circuit is required to open the ESS contactors if broken. The HVIL circuit travels through each HV system in such a way that if something should go wrong in HV circuit the HVIL circuit will break effectively closing contactors and isolating the battery pack from the rest of the vehicle. Although these safety measures are mandated. Other safety critical problems existed, and could only be tested or proven to fail while vehicle operation.

Studies say that time, cost, and quality are the three primary ways to measure a project's success [2]. Since this project has life critical operations, quality takes precedence over the other two measuring factors. Time and costs become secondary criteria while the quality of the resulting product is the focus. Even though quality was the primary focus the project would still fail if the requirements were not met on time. Thus, time was still taken in great consideration.

1.1.14 System Engineering

The electrical team was tasked with implementing a fully electric Chevrolet Camaro in three months with full functionality. To meet deadlines with minimal error, planning and collaboration was incorporated with regards to each component. Project management was required to ensure proper training and fulfilled goals. The methods used are also discussed.

Because safety was a high priority for vehicle design; the electrical design included features such high voltage inter-lock system (HVIL), emergency stop buttons, and a 12V disconnect switch. The HVIL circuit is required to open the ESS contactors if broken. The HVIL circuit travels through each HV system in such a way that would break the HVIL circuit effectively, in the event of a malfunction, closing contactors and isolating the battery pack from the rest of the vehicle. Although

these safety measures are mandated, other safety critical problems exist and can only be tested or proven to fail while the vehicle is operating.

Literature shows that time, cost, and quality are primary ways to measure project success [2]. Since this project has life critical operations, quality takes precedence over the other measuring factors. Time and costs become secondary criteria while the quality of the resulting product becomes the focus. Despite the focus being a quality product, the project would still fail if requirements were not met in time. Thus, time still had high consideration.

A systems engineering approach was also considered to increase the success rate of the project. Starting from the requirement phase to the end of the integration phase, the electrical team consistently contemplated the vehicle's overall goals by collaborating with the team's other technical groups, namely the mechanical and controls teams. To help streamline the process, requirement analysis and validation were combined and the results were reflected in the requirements specifications.

I. Stakeholder Requirements

The overall goal of electrifying the Camaro transform a vehicle identified as a “muscle car” to a PHEV that retains the quality and characteristics notorious to the Camaro brand. This overarching objective can be defined by a large number of sub-requirements given below. These requirements were developed by competition organizers, the overall team, and faculty involved. Identifying such requirements were fundamental to system engineering and integral to the project execution plan.

A. ESS

- 1.1.1 The system shall distribute energy to the HV electric inverters.
- 1.1.2 The system's current and voltage shall be monitored.
- 1.1.3 The system shall have communication via control area network (CAN) to the vehicle.

- 1.1.4 The system shall have internal CAN communication between each module.
- 1.1.5 The system's power distribution shall be controlled via contactors.
- 1.1.6 The system shall have a HV pre-charge resistor.
- 1.1.7 The system shall have high voltage interlock loop (HVIL) sent to it via a switch controlled by the main supervisory controller.
- 1.1.8 The system shall be separable via manual service disconnect (MSD).
- 1.1.9 The system shall have HVIL built into all of its HV vehicle interfacing connectors.
- 1.1.10 The system shall be electrically separable for installation purposes.
- 1.1.11 The system shall be electrically isolated from the low voltage system by a minimum of 500V/ Ω .
- 1.1.12 The system shall have a ground fault detector system to detect a current of 3mA from the HV bus to the LV chassis.
- 1.1.13 The system shall be designed to output 180 amps continuously.
- 1.1.14 The system shall be designed for a voltage potential of 380V.

B. Inverters

- 1.2.1 The system shall operate on a voltage range of 200V – 380V.
- 1.2.2 The system shall be capable of distributing a maximum of current 240 amps.
- 1.2.3 The system shall have CAN communication capability.
- 1.2.4 The system shall be resettable via a single digital line.

F. DC/DC converter

- 1.3.1 The system shall distribute up to 180 amps continuously.
- 1.3.2 The system shall be capable of supplying up 14.3V.
- 1.3.3 The system shall be controlled via CAN.

C. Electric Motors

- 1.4.1 The system shall be fully controlled via the inverters using analog inputs and outputs.

Front HV Disconnect Boxes

- 1.5.1 The system shall be capable of sustaining 85 kW of power for up to 10 seconds.
- 1.5.2 The system shall be capable of sustaining 63 kW of power for up to 36 hours.
- 1.5.3 The system shall allow isolation and ground fault testing via a HV connector.

D. Brusa Charger

- 1.6.1 The system shall charge the ESS within 8 hours.
- 1.6.2 The system shall communicate via CAN.
- 1.6.3 The system shall use analog inputs to charge the vehicle.
- 1.6.4 The system shall be capable of supplying between 200V and 380V.
- 1.6.5 The system shall be capable of distributing 12 amps to the ESS.
- 1.6.6 The system shall be protected via a HV fuse.
- 1.6.7 The system shall be configurable via serial communication.

E. Supervisory Controller

- 1.7.1 The system shall have more than one CAN channel
- 1.7.2 The system shall have analog inputs.
- 1.7.3 The system shall have digital outputs.
- 1.7.4 The system shall allow no more than 70 mA of current flow.
- 1.7.5 The system shall be powered with a 12V DC supply.
- 1.7.6 The system shall use no more than 12 amps under full load.
- 1.7.7 The system shall be electrically enabled to enter a sleep mode and a wake mode.

G. Engine Control Module

The engine control module (ECM) was given completely assembled, mechanically, electrically and software installed. The controller however, had to be integrated into the vehicle. As a result, requirements were not created for this sub-system.

H. Power Distribution Box

- 8.1 The system shall be controlled via CAN.
- 8.2 The system shall distribute up to 30 amps of current.
- 8.3 The system shall operate on a 12V DC source.
- 8.4 The system shall have four output PWM channels.

1.1.15 Architecture Design

Sub-systems of the electrical system were created to simplify the design and the implementation process. The sub-systems were divided into high voltage, low voltage and communication sub-systems. Every component was provided by an automotive components manufacturer, except the disconnect boxes and power distribution module. As a result, harnesses were created to fulfill the requirements for the given components and complete designs were done for the two built subsystems.

To further simplify the designs, each subsystem was designed separately. The HV sub-system consists of each component that utilizes high voltage. These components include the Brusa charger, the ESS itself, the front distribution disconnect enclosure (DDE), the two inverters and the electric motors.

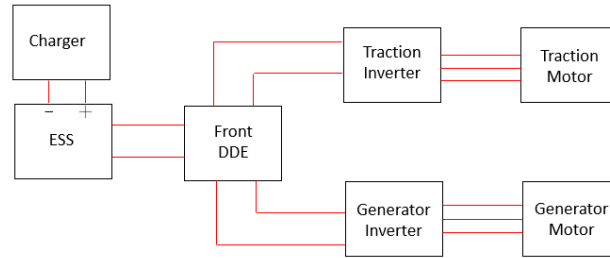


Figure 12: HV Sub System Components

The LV sub system consists of the DC/DC converter, the 12v battery, the stock fuse box interface, the BVM, the ECM, the supervisory controller and the control circuit for the Brusa, inverter and the motors are included. The third subsystem is the CAN bus system. The sub system consists of the vehicle added CAN bus. Each

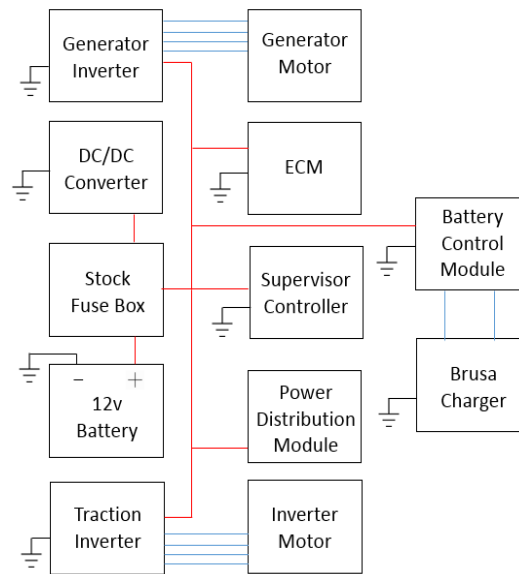


Figure 13: LV Sub System Components

CAN bus interfaces with the supervisor controller, which then correlates the messages to the vehicle stock CAN bus.

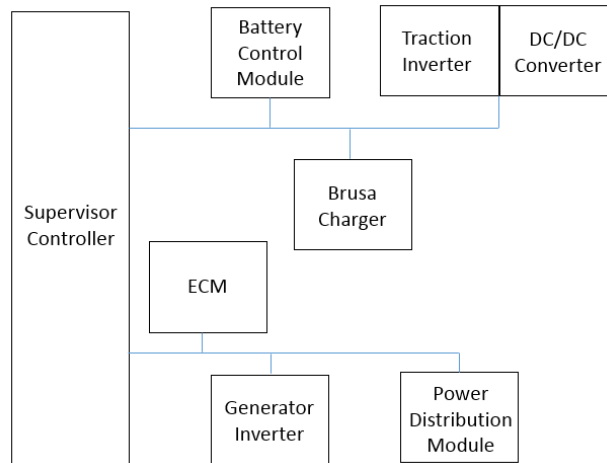


Figure 14: CAN Bus Sub System Bus Connections

With the help of the block diagrams above, circuit designs were created with wire sizes and pin numbers. Using both the schematics and the block diagrams, wire harnesses were created. The clear independence of each sub-system helped with understanding of the sub-systems architectures. After designing the schematics and wire harnesses, parts were bought to prepare for implementation and integration. Parts were bought on a sub-system by sub-system basis

1.1.16 Electrical Implementation

After each sub-system was determined, testing of each component was conducted to prove rudimentary functionality as specified by the manufacturer. The implementation process was completed with the controls and mechanical team to test each component physically, if necessary, electrical input and outputs. A similar implementation plan was created for each subsystem, with some-sub-systems broken down to more sub systems.

In each sub-system, splices had to be made. Many splices had to be used within the implementation process to transform a gasoline vehicle into a hybrid electricity variety. With quality as a key factor in the system design, a basic analysis was done on butt splices and solder joints. The idea behind a good electrical splice is that the joint should not be the weakest link once implemented. Butt splices

with wires less than 18 gauge have a stronger mechanical connection than smaller wires. However, butt splices cover less surface area than a solder joint.

Research was done on the various splices available. The most important factor in the choice of splicing methods was reliability over a 4000 mile driving range. The second factor was time and convenience. Solder joints were the fastest method for implementation when the component and harness are in inconspicuous locations. However, mechanical splices were the most reliable. Because the vehicle is only required to travel at most 4000 miles' solder was considered assuming the joint was soldered correctly. Research shows that solder joints are most effected by temperature and thermomechanical fatigue [3]. Based on the equation below temperature aging has an exponential effect on solder joints merging two metals that are different from the actual solder material,

$$x(t, T) = x_0 + Atn * \exp\left(-\frac{Q}{RT}\right) \quad (3)$$

Where x is the total intermetallic thickness (mm), t is the time (s), x₀ is the thickness of the intermetallic in the as-solder condition, at t =0, A and n are constants, R is the universal gas constant, and Q is the apparent activation energy for a particular growth process. Multivariable Linear regression of intermetallic growth data can be used to determine the actual values of A, n and Q.

We can see, from this equation, that the temperature has exponential effect on the solder joints. To minimize temperature effects on each harness that contained solder joints, these harnesses were routed away from the engine and wrapped with thermal insulation to help heat convection. Research also shows that vibration from an automobile's engine has little effect on solder joints if implemented correctly. Acoustic areas within the vehicle however, can pose a problem due to resonance frequencies. For the work conducted solder joints were used primarily within the engine

bay to increase productivity and convenience, because of the vehicles short operating life span. As mentioned earlier, thermal preventative measures were taken into account.

The HV sub-system was separated into two phases. The ESS being its own phase and the inverters, motors and the front DDE being the second phase. The ESS had a higher probability of failure, particularly because of interfaces between the mechanical, controls and electrical teams. Therefore, it was created first to ensure proper functionality. Initially, the work flow process of each sub-system was planned out starting with the ESS. Required tools were bought and secured for the HV work along with the required personnel to complete the tasks. Both mechanical and electrical engineering students were involved in the ESS build. While building the ESS isolation and electrical connectivity were the primary concerns of the team due to physical design of the system. Electrical HV insulated tape was used in areas where clearance was less than minimum distance for a 350V system. Finger proofing was used in the event of accidents involving tools dropping or touching that would cause short circuit or electric shocks. The implementation process took over 7 days, 8 hours per day, to fully complete the ESS. Problems arose in the first phase of the plan regarding some parts, namely nuts and bolts. A charging problem occurred because the current sensor was wired backwards.

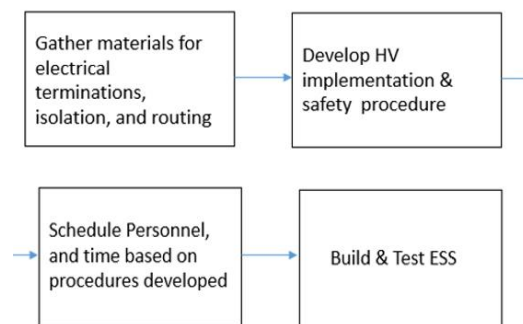


Figure 15: ESS Implementation plan

The second phase is larger with an even higher probability of failure. This phase was organized into several sections to simplify potential troubleshooting and determining functionality. The first

subsystem involved the ESS LV wire harness which consists of the battery control module, a current sensor and a HV control switch. Within this phase, the team accounted for too much extra wire which caused a physical implementation problem. The second phase of the LV sub system was the charger wiring, which had no electrical issues after testing on component basis. The third phase was then the inverters, DC/DC converters and the electric motors. Within this phase there existed no problems during component testing.

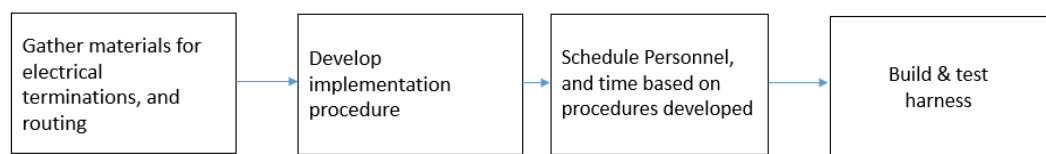
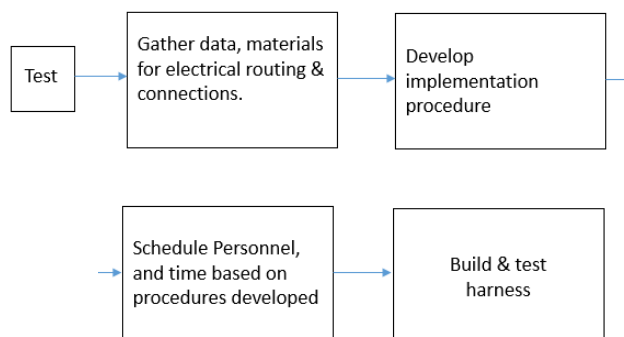


Figure 16: LV ESS Implementation plan

The engine control module was given its own phase due to the substantial number of connections and inability to test unless cranked and running. This implementation phase slightly differs from the other phases due to the complexity in functionality and failure points. For this phase, the stock ECU was first tested to determine optimal functionality and behavior based on the manufacturer wiring and documentation. After determining the intended behavior of the ECU, material was gathered for implementation and wire routing. A strenuous implementation process was conducted that took approximately a week to complete for testing. Problems arose with regards to the wire



routing.

Figure 17: LV Engine Implementation Plan

Finally, the supervisory controller was implemented in parallel with every subsystem to avoid potential confusion due to wire cluster and bundles. The implementation plan was similar to all of the other plans, where material was gathered to enable functionality for its corresponding component being implemented. An error occurred due to untrained personnel working on the component.

The third subsystem created was the CAN Bus subsystem. This subsystem was created in a single phase. The data and research conducted in past months by the electrical team allowed for a simple implementation with minor problems. Each component on the CAN bus was easily separable from the CAN bus, which made the troubleshooting and testing feasible. The problems that arrived during the testing phase was due to a node being connected to non-CAN bus wires. In one day, the CAN bus was fully functional. After testing and continuous tampering with the vehicle, solder joints came loose. This method of creating joints was reevaluated and changed to either crimps splices or connectors due to the high dependability of the communication bus within the vehicle.

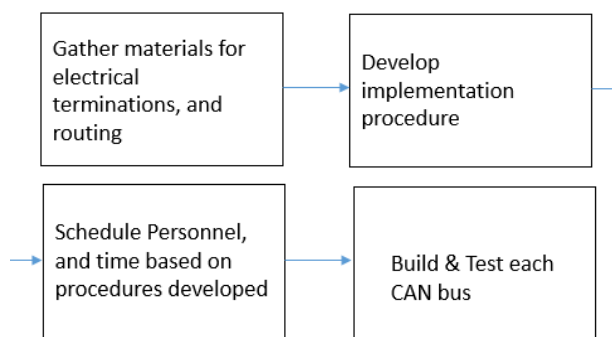


Figure 18: CAN bus Implementation Plan

1.1.17 Integration

The integration process is the process of assembling the constituent parts of a system in a logical, cost effective manner, comprehensively check system execution with a full functional checkout.

The implementation phase is a form of integration, but only consists of implementing component and sub-system integration and not the system as a whole. Each system is fully integrated electrically primarily over the CAN bus and mechanically based on the mechanical team goals'. Once the sub-systems were all integrated, basic power and I/O checks became the main task for the electrical team, while the controls team took over to make the vehicle fully functional. Once the components were fully integrated, CAN messages were sent to determine basic functionality. To completely validate the systems requirements, vehicle driving was done while monitoring how each component functioned while the vehicle was driving.

1.1.18 Testing

Testing involved a two-stage driving process. The first stage with the vehicle under no load and the second phase with the vehicle under full vehicle load at low speed, less than 35 mpg. The vehicle was placed on a lift where both wheels were off of the ground and the wheels were span in both forward and reverse. The second stage consisted of the vehicle driving around in circles no greater than 35 mph. After the three-month period passed, the vehicle was tested at high speeds (at least 60 mph).

1.1.19 Verification

During the first stage, each requirement was capable of undergoing the verification process except for the charging requirements, the maximum electrical power output, and the power distribution box PWM outputs. The CAN messages required to control the power distribution box was unknown during the verification process. More verification occurred after the initial planned phases where the vehicle drove at high speeds. Each requirement was looked at one at a time to determine if the system was built correctly.

1.1.20 Validation

Validation was a more strenuous process that is an ongoing process between all technical teams. In this stage, the team tried to determine if the right system was being built. Requirements were revised based the controls teams and the mechanical feedback in order to address real world needs.

1.1.21 Transition

To ensure that the electrical system continues to perform reliably meeting all requirements and to increase longevity, an optimization plan has been created. The 12V battery, the DC/DC converter, the power distribution unit, and controllers will be the primary devices under observation. Each component mentioned was added or can be affected by the teams added components, so must be analyzed. All data collected will be collected via an mBed controller. These devices also play critical roles in vehicle's operation. The goal of the optimization plan is to help the electrical team determine how well the electrical system is built.

Chapter 2 Literature Review

The literature review focuses on common electrical problems, how to compensate for them and ways to simulate a realistic electrical system based on manufacturer data. Electrical problems with respect to power systems, communication systems along with issues involving semiconductors such as micro controllers.

2.1 Power System Issues

Many of the problems that appear in real world electrical circuits come from power supplies [4]. Power supplies can cause noise and spurious oscillations that can lead the designer towards tedious glitch hunts [4]. Clean supplies are essential for low noise, stable, and clean designs and they are not difficult to achieve [4]. Noise can be defined as an unwanted signal that interferes with the communication or measurement of another signal [5].

Documentation shows several common electrical issues that arise within a power system circuit. These problems lead to equipment failure, downtime, software and data corruption. The Institute of Electrical and Electronics Engineers (IEEE) provides methods for safeguarding equipment using their standards for describing power quality disturbances. IEEE has defined seven categories of power quality problems, namely, transients, interruptions, sag/under voltage, swell/overvoltage, waveform distortion, voltage fluctuations, and frequency variations.

Transients can be the most damaging type of power disturbance [6]. Transients can be broken down into two categories, impulsive and oscillatory. Impulsive transients are sudden high peak events that raise the voltage and /or current levels in either a positive or a negative direction [6]. Impulses are generally categorized by speed such as fast, medium, and slow. An impulsive transient is caused by lightning, poor grounding, switching of inductive loads, utility fault clearing and electrostatic discharge (ESD). As mentioned earlier, this can cause physical equipment damage and data loss. The most common protective methods pertain to the removal of ESD. A filtering circuit or device

is commonly used for such applications [6]. Oscillatory transients are the second type of transient and is the most common. It is defined as a sudden change in the steady state condition of a signal's voltage, current or both. These type transients occur due to inductive or capacitive loads being switched on and off [6]. All electrical circuits have some form of inductive and capacitive properties that briefly energizes in a decaying form [6]. This problem can be solved using the same method mentioned for impulsive transients. The basic mechanism behind supply line transients is shown in Figure 19. The transient voltage produce can be expressed as

$$v = L \frac{di}{dt}$$

(4)

Because of the contact bounce, transients are generated whether the switch is being opened or closed.

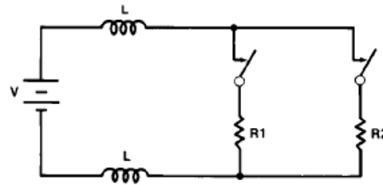


Figure 19: Supply Line Transients

An interruption is defined as the complete loss of supply voltage or load current [6]. The duration of the voltage or current loss can be categorized as instantaneous, momentary, temporary or sustained. Causes of interruptions are lightning strikes, accidents/component damage, fuse blowing, and line faults. The solutions to these problems vary in effectiveness and cost [6]. A typical effort should go into eliminating or reducing the likelihood of potential problems.

Sag is a reduction in voltage. Sags are generally caused by system faults and is typically due to switching on loads with high currents with respect to other components. A motor can draw up to

six times its running current, or more, while starting. With large electrical loads, such as this will likely create significant voltage drop to the rest of the circuit it resides on [6]. The damage being caused by sags is not apparent until the results are seen over time. A solution to this problem would be to use a separate circuit to supply the heavy loads. Under voltage are the result of long -term problems that create sags [6]. Under voltage can cause overheating within motors and can lead to the failure of non-linear loads. Constant under voltage is sign of serious equipment fault. An under-voltage problem can be solved similarly to a sag problem.

A swell is the reverse of a sag [6]. A common source to this issue is a sudden load reduction. This can cause semiconductor damage in electronics, degrading of electrical contacts and degradation of insulation. Signal conditioning is a common solution to this problem. Swells may not be apparent until their results are seen [6]. Over voltages can be the result of long-term problems that create swells. This can cause unnecessary blowing of fuses downstream as well as overheating and putting stress on equipment.

Waveform distortion has five primary types, namely, DC offset, harmonics, interharmonics, and notching. DC offset is a problem with AC distribution systems. Harmonic distortion is the corruption of signals at frequencies that are multiples of the fundamental frequency [6]. Harmonic filters can help with this problem. Interhamonics are a type of waveform distortion that are usually the result of a signal imposed on the supply voltage by electrical equipment such as static frequency converters, induction motors and arcing devices [6]. The most noticeable effect of interharmonics is visual flickering of displays and incandescent lights, and possible heat and communication interference. Finally, notching is periodic voltage disturbance caused by electronic devices, such as variable speed drives, light dimmers and arc welders under normal operation.

The six-power problem quality is voltage fluctuations. Voltage fluctuations is a systematic variation of the voltage waveform or a series of random voltage changes, of small dimensions between 95 to 105% of nominal voltage at a low frequency, typically below 25 Hz.

The final power quality issue is frequency variations. Frequency variations generally only exists in AC systems. Voltage imbalance is not a type of waveform distortion, but it is important when assessing quality problems. Once again, this problem generally effects AC systems due to the different voltage sources that arise particularly in 3-phase systems.

Besides the seven common problems mentioned above, there exist other electrical problems that exist within electrical systems. Many of which not related to the scope of this research. However, there are two more issues worth mentioning, namely thermal noise, grounding noise and electromagnetic noise. Thermal noise is generated by the random movements of thermally energized particles [5]. As the temperature in a conductor increases, the electron move to higher energy states and the random current flow increases [5]. Electromagnetic noise exists in virtually every electrical device that generates, consumes or transmits power. As a result, they are all a potential source of electromagnetic noise and interference for other systems. Common sources of electromagnetic noise are transformers, microwaves, ac power lines, relays, motors and motor starters [5].

Electric and hybrid vehicles will produce more EMI than the conventional internal combustion engine vehicle [7]. Electric vehicles use high power electronics to drive the vehicle which produces high-level low frequency EMI [7]. Research shows that magnetic tests demonstrate twisted paired wires is a more effective means of reducing magnetic noise than installing wire in conduit for use as magnetic shield [8]. Also, nonferrous shields have no effect on reducing magnetic noise [8].

2.2 Noisy Automotive Environments

Noises in digital systems produce software upsets, programs jump to random locations in memory [9]. The signal lines can be affected by such noise, but the supply line is more prone to noise than the signal lines. The automotive environment, in ordinary operations, the 12v power line can

produce transients of $\pm 400\text{v}$. A DC/DC switching power converters are natural generators of noise [10].

It is difficult to produce an automotive environment during a bench test. Noise problems tend not to show up until the system is installed and operating in its intended environment. After implementation, a few minutes or hours of normal operation the system may begin to fail. A reset may solve the problem, but sometimes a physical disconnection is required [9]. The system may then begin to operate as normal. Most times the fault cannot be induced or replicated, which makes it difficult to determine. The fault may show again after a few seconds, or a few minutes, or even a few days later, but still unpredictably. Randomness is one form of electrical noise problems [9]. Some noise problems can produce faults periodically. The more difficult it is to characterize an upset as a cause and effect, the more likely it is to be a noise problem.

The name given to electrical noises other than those that are inherent in the circuit components (such as thermal noise) is electromagnetic interference (EMI) [9]. There are many types of EMI problems. EMI problems come from motors, power switches, fluorescent lights, electrostatic discharges, etc. Arcs and sparks occur in automotive ignition systems, electric motors and switches [9].

2.3 Ground Noise

Reliability in low voltage systems depends on many factors, including proper system and equipment grounding [11]. Currents in ground lines are another source of noise. Noise within ground lines is referred to as ground loop problem. The basic ground loop concept is shown in Figure 20. A ground loop is the difference in potential between ground points. If two or more ends of a wire chassis grounded at various locations, the difference between the two ground points can drive significant currents through the wires [9]. The term is used to refer to unwanted currents in a ground line.

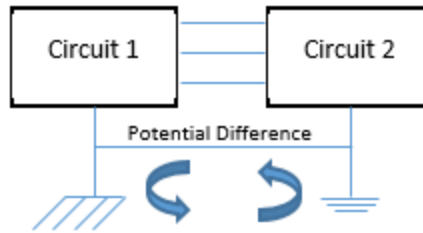


Figure 20: Basic Ground Loop

The automobile presents an external hostile environment for electronic systems. There are three main parts to consider:

1. Temperature extremes from -40°C to $+125^{\circ}\text{C}$, under the hood or $+85^{\circ}\text{C}$, in the passenger compartment.
2. Electromagnetic pulses from the ignition system
3. Supply line transients

The operating temperature of a microcontroller needs to be greatly considered before utilizing inside of an automobile. Although a IC is designed for different product grades such automotive vs industrial, this doesn't mean that an industrial chip can't operate effectively within an automobile. The IC grade simply specifies the level testing conducted on the chip [9]. According to Intel, ignition noise and CB radios are probably the least likely to cause severe damage to an IC [9]. In a poorly designed system ignition EMI might cause software upsets, but not destroy a chip. The transients within automobiles tend to be the biggest cause of failure [9].

2.4 Measurement

The automotive industry sensor measurement can be classified into the categories, monitoring of processes and operations, control of processes and operations, along with experimental engineering analysis [12]. Conducted output noise voltage measurements are difficult to make even under the best conditions [10]. An oscilloscope has a finite ability to reject common mode signals, and these signals can be worsened by using long ground leads on the scope. The ground leads on the scope

have an inductance not present on the signal lead [10]. Leads length, including the ground must be as short as possible to reduce the pickup of radiated noise. To determine common mode noise, tie the scopes measuring probe to the ground lead of the scope and connect the probe to source, found or positive rail. If there is noise even though the two leads are tied together there is common mode noise. To filter the conducted mode noise, capacitors are sufficient [10]. When determining the harmonic distortion levels, a harmonic filter design, or transient waveform analysis, the proper choice of instrumentation, measurement technique, and analytical tools can make a difference between a well-engineered solution to complex problem and an expensive failure [13].

2.5 Simulating a Lead-Acid Battery

Lead-acid batteries are used within automotive vehicles to sustain the vehicles accessory loads and to supply the starter motor within fully gasoline powered vehicles. Electrical system simulations are heavily dependent on the battery sub-model, which is the most complex component to simulate [14]. Studies show that methods for modeling lead acid batteries are typically unclear, difficult, time consuming, and expensive [14]. There have been many proposals for lead acid battery models. One of the models is the Thevenin equivalent circuit. An improvement upon the Thevenin model is a linear electrical battery model shown in Figure 21 [15]. This model does not take into account thermal dependence and uses different sets of element values to model the battery at different states of charge. Any lead-acid battery can be modeled by using the manufacturer specifications and experimental results [15]. The manufacturer includes in the datasheet the evolution of the discharge characteristics curve.

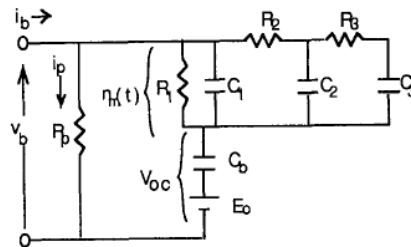


Figure 21: Linear Electrical Model

2.6 Simulating Loads

The accurate assessment of load modeling for this research is important for deductive reasoning purposes. It remains a challenge to properly develop load models which can be used with confidence in studies. It is clear it is impossible to obtain a precise model of system loads since the loads are very complex and continually changing [16]. Therefore, a practical means must be used to capture the dominant characteristics of the load and sensitivity analysis used to judge the effects of variations in the model [16].

Depending on the stage of development of the vehicle, the available information about the component and systems varies and so, consequently, do the simulation models. There are various ways of dealing with a lack of important data. For previously used components, there may be existing models that can be used instead. If this is not the case, models can be calculated from component parameters derived through measurements [17]. If it is a new component and the potential suppliers are known, preliminary data can be requested from them. The supplier may even provide an encapsulated model of its component. If suppliers are not known, comparable components and their models can be applied with appropriate adjustments. The respective component experts are involved in the process at every stage. With their expertise, it is also possible to develop the right test cycle to determine the maximum current load [17].

Modeling vehicle noise can be difficult. The noise in a car is non-stationary, varied, and may include quasi-periodic noise from the car engine and the revolving mechanical parts of the car. Noise may come from the surface contact of the wheels and the road surface [5]. The vehicle's air flow from windows and air duct may cause noise along the passing and overtaking of vehicles [5]. The characteristics of vehicle noise varies with speed, the road surface conditions, the weather,

and the environment within the car [5]. For this thesis, the simplest form of noise modeling will be used, which is estimating the noise statistics from the signal-inactive periods [5].

2.7 Lead Acid Battery Charging

Research shows that there are several factors that can affect the battery's life. Some of the main factors that affect battery life are float voltage accuracy, frequency of discharges, number of discharges, maximum discharge rate, depth of discharge, end voltage limit, the operating temperature, and the amount of ripple current and voltage allowed, during charging as well as discharging [18].

Most electric vehicles (EV's) are power by 12v batteries. Battery charging techniques includes SOC estimates, optimization of charging control, reduction of charging time, and series connected method [19]. Constant current charging is a simple charging method that uses constant currents for battery charging and the charging currents for the series connected batteries are equal. This will, however, degrading of the battery if overcharged [19]. Constant voltage charging is the most common used charging method for lead acid batteries [20]. With this method, each individual cell share the voltage and equalize the charge between them [20]. However, with a single fixed voltage, it is impossible to properly balance the requirements of a fast charge cycle against the danger of overcharge [20].

Battery life is depended on three factors, namely, temperature, aging and number or depth of discharge cycles. The ambient temperature of the cells is a major factor in the lifecycle of the battery system [21]. Cells will degrade with age; just using batteries causes them to age. Automotive batteries are more susceptible to aging because they tradeoff lower maintenance for lifetime [21].

2.8 Voltage Ripple and DC/DC converters

Several methods exist to achieve DC-DC voltage conversion. Each method with its specific advantages and disadvantages. The most elementary DC-DC conversion method are linear voltage

converters. They achieve DC-DC voltage conversion by dissipating the excess power into a resistor, which makes them voltage dividers [22]. The disadvantage of this method is that they are not ideal for power conversion efficiency and the voltage is not stable over a large range of voltages inputs. However, the implementation design is simple [22]. Charge pump and inductive type DC-DC converters are similar in topology [22]. They both require energy storing passive devices and switches to alter the connections between the input and output [22]. This is why DC-DC converters are called switching power supplies. Charge pump utilizes capacitors while inductors utilize inductors [22]. Each non-linear DC-DC conversion falls under different converter types, namely, buck, boost and buck-boost converters [23]. All DC-DC converters are highly efficient, in practice, efficiencies of 70% - 95% are obtained [23].

Output ripple and switching transients are two undesirable signals on a switching regulator's output. The output ripple is the ac output voltage residue and is coherently related to the switching operation of a switching regulator [24]. Every switching power converters with a DC output voltage will contain some ripple and noise component on the output [25]. Switching transients are high frequency oscillations that occur during switching transitions. Its amplitude is expressed as a maximum peak-peak value [24]. This is difficult to measure accurately since it is highly dependent on the test setup [24].

Battery manufacturers recommend that under normal float charge conditions, battery ripple root mean square voltage must be limited to less than 0.5% of the DC voltage applied to the battery [26]. Higher voltages can create heating effects on the battery because of constant charging and discharging of cells [18]. Even if the battery voltage is kept within this threshold, it is still possible for the current ripple to damage the battery due to the internal battery resistance [26]. Beyond the concern of heating due to excessive AC ripple current, there is the additional concern for battery gassing and dry out due to excessive charging voltages [27].

Chapter 3. HV Optimization

The HV system had no operational problems since its implementation, except for the a/c compressor which was corrected by swapping the leads. Although there are ways to optimize the HV system by evaluating the system itself and improving the physical implementation, this method of optimization was avoided. The safety hazard involved in a potential error that could result in a detrimental event after re-implementing a circuit was not worth the risk.

The optimization performed on the HV system was performed via software seen that most the apparent issues related to control strategies. Thus, the electrical team created models that could simulate the HV vehicle losses, where assumptions were made to simplify the simulation. The results of the simulations were then compared to the actual vehicle data and compensated for where necessary. Because the electrical team was not involved in the team's controls strategy implementation, only a thermal analysis was done. The electrical team could in this regard help optimize the HV system by working with the controls team determine a control strategy that would regulate a range of heat.

3.1 Operation and Analysis of the Inverter

The inverter utilizes insulated-gate bipolar transistors (IGBT's) to switch the load off and on at frequencies between 10Hz – 30 KHz, data given by manufacturer. Diodes are placed in parallel with transistors to protect the circuit from counter electromotive force. As power is dissipated through the entire power module, heat develops from the IGBT's, the diodes and the surrounding circuit board and housing. In this paper, only the conduction heat interaction between the IGBT's and diodes are considered.

Theoretically, an ideal IGBT would have no resistance, hence no power consumption. For a real switch, there are losses due to conduction and switching. The conduction losses occur when the IGBT is conducting and the switching losses occurs when the IGBT switches on and off. Losses

within the IGBT produces heat, hence acting as heat source and increasing the device's junction temperature. This phenomenon is called self-heating.

The power losses of the IGBT produce heat which in turn affects the voltage and current output of the transistor as shown in Figure 22. A thermal model is required as a result of this relationship to yield the inverter losses.

There are several ways to create a thermal model, two popular methods being the finite element method (FEM), and the finite difference method (FDM), which are both numerical methods. There are also analytical methods that are mathematically complex. In the paper RC, thermal networks will be used to create a thermal model. This method can be used to describe 1-3 D [2, 3] problems.

For heat conduction in a homogeneous isotropic material, the conduction is described as,

$$\nabla \cdot (k(\nabla T)) = \rho c \frac{\partial T}{\partial t} \quad (5)$$

Where k is the thermal conductivity, ρ is the mass density, c is the specific heat. T is the temperature.

IGBT as a vertical power device, the thickness L is small than other dimensions. A one-dimensional conduction process is therefore assumed [4]. The thermal characteristics of silicon chip is also independent of temperature. The above assumptions simplify the equation given above to,

$$k \frac{\partial^2 T}{\partial x^2} = \rho c \frac{\partial T}{\partial t} \quad (6)$$

Where x denotes the coordinate in the direction of heat propagation.

The RC network description of the thermal property of a device is based on the similarity between the previous equation and the differential equation of a transmission line [5],

$$\frac{\partial^2 V}{\partial x^2} = C'R' \frac{\partial V}{\partial t}$$

(7)

Where C' is the capacitance per unit length, R' is the resistance per unit length of the line. For an IGBT, we can use a transmission line equivalent circuit as shown in Figure 23.

The parameter value of the lumped thermal RC network are found by segment of the device into substructures as shown in Figure 23. Each substructure will correspond to a different layer of material in the IGBT module see Figure 22 [6]. The equations below are then used to estimate the thermal resistors and capacitors' of each layer (substructure),

$$R_{th} = \frac{d}{A.k}$$

(8)

$$C_{th} = c * \rho * d * A$$

(9)

where d is the length along the heat conductive direction, A is the area perpendicular to the heat conduction direction.

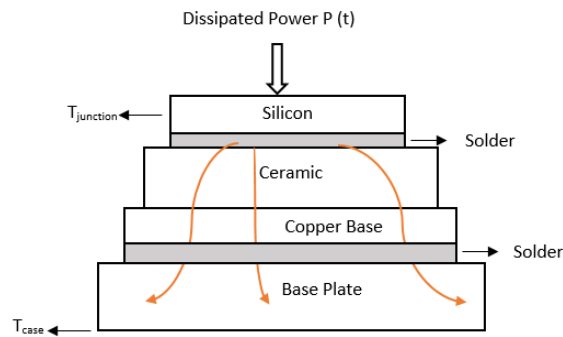


Figure 22: Physical Structure of Module

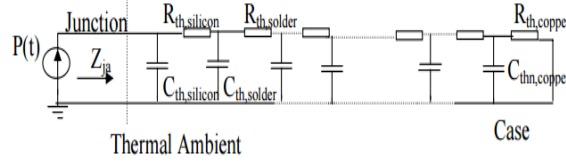


Figure 23: Thermal RC network

Using basic circuit analysis we obtain the impedance in the form of a transfer function,

$$Z_{jc}(s) = \frac{1}{sC_{th1} + \frac{1}{R_{th2} + \frac{1}{sC_{th2} + \dots + \frac{1}{R_{thn}}}}}$$

(10)

In order to model the IGBT using this method an IGBT was chosen based on the traction motor power capabilities such as maximum output current and voltage. By doing this a transient thermal impedance curve, based on a datasheet, from the junction to the case to the IGBT module could be used to obtain,

$$Z_{jc}(s) = 0.001 \cdot \left(\frac{1.25/\sqrt{0.003}}{s + 1/\sqrt{0.003}} + \frac{6.15/\sqrt{0.05}}{s + 1/\sqrt{0.05}} + \frac{2.6/\sqrt{0.1}}{s + 1/\sqrt{0.1}} + \frac{3/\sqrt{0.95}}{s + 1/\sqrt{0.95}} \right)$$

(11)

this reduces to,

$$Z_{jc}(s) = \frac{0.56882 \cdot s^3 + 65.659 \cdot s^2 + 766.16 \cdot s + 912.28}{s^4 + 364.39 \cdot s^3 + 10582 \cdot s^2 + 77404 \cdot s + 70175}$$

(12)

This transfer function is used in the thermal Simulink model as a function in a function block.

3.2 Inverter Electrical and Thermal Module

The first analysis on the traction inverter is done assuming a constant pedal position is being applied at approximately 60 -65 mph. This speed generally corresponds to currents between 70 – 110 amps continuously.

The traction inverter is simulated in Matlab's Simulink program using 6 IGBT's all in parallel with diodes with inductors and resistors acting as the motor. A pulse width modulation (PWM) generator is used to switch the gates of the IGBT off and on at 20 kHz with modulation frequency of 100 Hz and modulation index of 0.8. The model is given in the appendix A 1: HV Inverter with Motor Model.

A thermal model is created in Simulink using the transfer equation given earlier. The thermal model uses power inputs from the diodes and the IGBT used in the inverter. The thermal model outputs a corresponding temperature as shown in Figure 24.

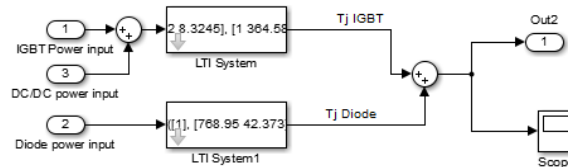


Figure 24: Thermal Model

3.3 DC/DC converter Electrical and Thermal Module

The DC-DC converter is capable of outputting 2.55KW, with a maximum current output 170 A and voltage output of 15 V. It is built into the same package, a power electronic module (PEM), as the inverter circuit. The power losses from the dc/dc will then affect the inverter thermal properties. This model assumes worst case thermal interaction between the dc/dc and the inverter because the internal makeup of the PEM is not known. The model is combined with the inverter thermal model

above in Figure 24. The heating affects is fairly small due to low power output of the dc/dc converter compared to the inverting circuit and the 90-95% efficiency of the buck converter circuit.

The dc/dc converter circuit utilizes an inductor to create a buck circuit. A switch is pulsed at 1000 times a second with a pulse width of 20. The first resistor in the circuit acts as the load and the second as heater to create the respective efficiency given by the manufacturer. See the model in Figure 25.

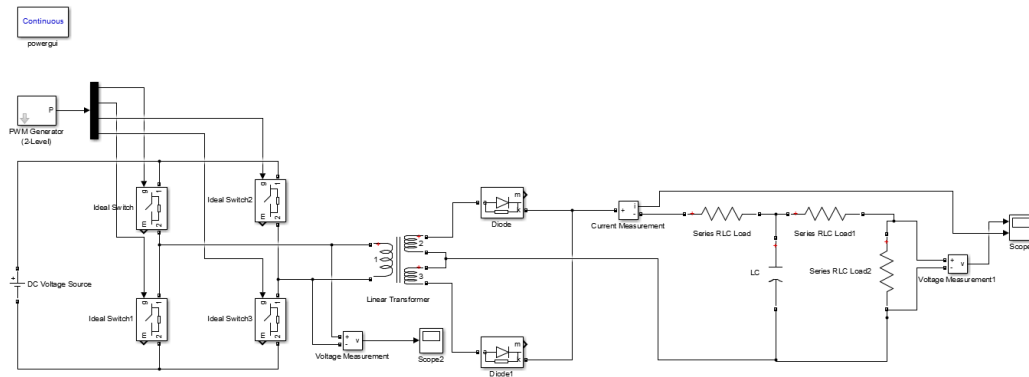


Figure 25: DC-DC Converter Model

3.4 Asynchronous 3-phase Electric Motors

The electric motor efficiency is given based on rpm and torque by the manufacture. Having the vehicle simulated at approximately 60 mph an estimated efficiency figure level can pulled from the datasheet given. The resistor in the circuit acts as a heat dissipating element to produce the respective power output across the motor. This model; can be seen with the inverter model in appendix A1.

3.5 Inverter data Analysis

The inverter model produces current outputs going to the 3-phase motor. The 3-phase current is shown in Figure 26. Using two motors the battery current of 80 A is divided two giving which would yield the current below.

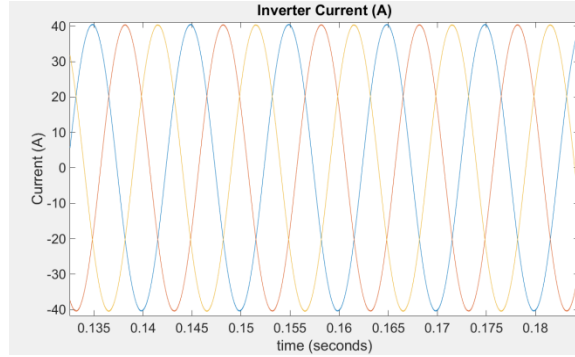


Figure 26: Inverter Current

The thermal model produces temperature outputs for the IGBT junction temperatures as shown in Figure 27. The IGBT has an initial temperature of 25 degrees Celsius. The power losses fed into the model gradually increases the junction temperature to steady state value. Based on the data in Figure 27, we can see that the temperature increases rapidly to roughly 30⁰ C before reaching a controllable state.

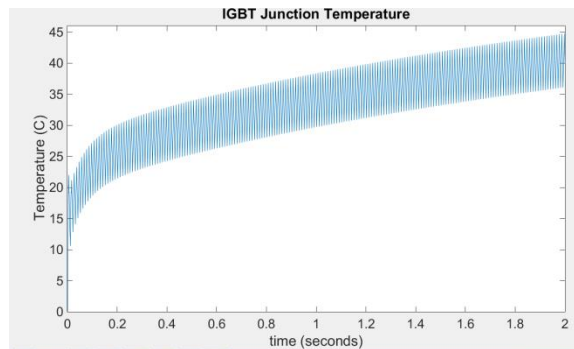


Figure 27: Junction Temperature Output of IGBT's

3.6 DC/DC Data Analysis

The DC/DC is a simply model used to help give a more realistic thermal model for the PEM. The manufacturer data sheets states that the DC/DC converter within the vehicle is capable of supplying 2.5kW, equivalent to 14.7v and 180 amps. In Figure 28, the voltage output is given as a function of time. And in Figure 29, the current output is given. After taking actual current measurements

from the DC/DC converter, it was determined that currents between 30-60 amps is typical current draws from the low voltage systems within the vehicle when driving depending on the components used.

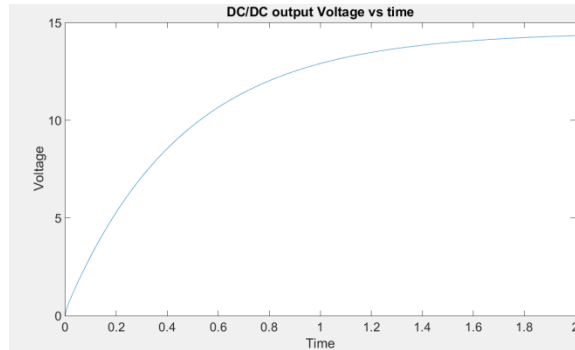


Figure 28: DC/DC Voltage output - 14.3V

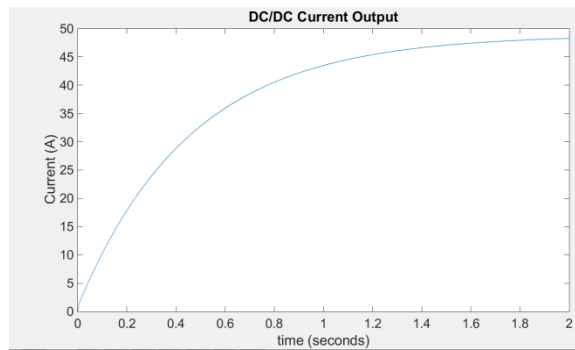


Figure 29: DC/DC Current Output

3.7 Overall System Analysis

All powertrain components are considered within the model. The traction inverter, and electric motors. Assuming highway speeds of 60 mph, the model yields losses within the inverter and at 60 mph data is given on the motors operational efficiency at equivalent rpm and output torques. The overall system model is given in Figure 30. Power flows from the ESS to the inverter and DC/DC converters. From the traction inverter to the motors. Both the inverter and the DC/DC converter affects the thermal system and the thermal system itself affects both converters power output.

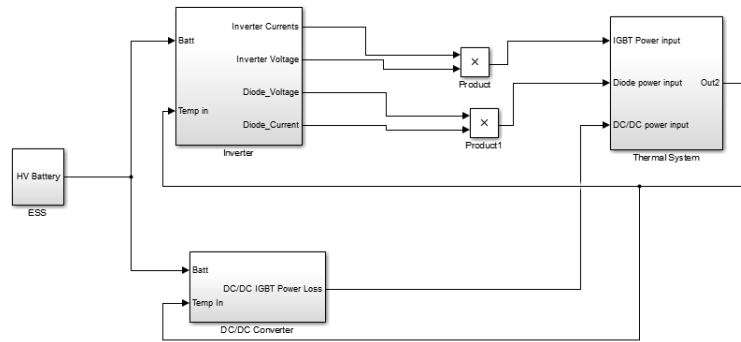


Figure 30: Overall Model

The instantaneous power loss of the inverter's IGBT is given in Figure 31. This calculation was calculated using the IGBT voltage drop and the current flowing through both the diode and the transistor, which occurs when the IGBT switches off and on between transition states.

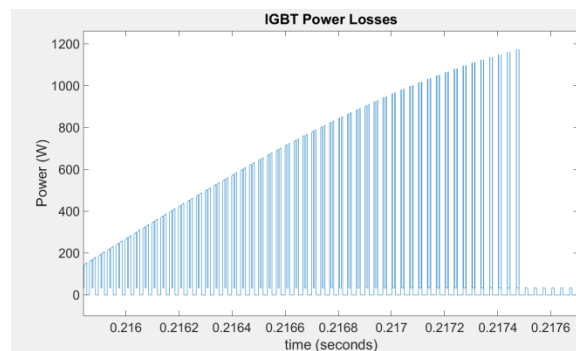


Figure 31: IGBT Power Losses

Based on the manufacturers' data, the motors should operate at an efficiency of roughly 75% efficiency with an rpm of 1500 and a torque of 120 Nm with a coolant temperature of no more than 65⁰ C. The power loss of the IGBT is averaged in the calculations below.

The overall powertrain can now be calculated as,

$$\text{ESS Power Out} = 350\text{v} \times 75 \text{ amps}$$

$$= 26,250/2 \text{ W}$$

$$= 13,125 \text{ W}$$

the division by 2 occurs due to having the load split equally between 2 motors.

Power Loss = Inverter Power loss + Motor Power Loss

$$= 592 \text{ W} + 13,125 \times 0.25 \text{ W}$$

$$= 3873.25 \text{ W}$$

$$\text{Efficiency} = 7746.5 / 26250$$

$$= 0.705$$

The vehicle has a powertrain efficiency of 71% at high speeds.

3.10 HV Conclusion

The model yields power outputs based on thermal effects of the PEM. With this and the manufacturer information on the electric motors, the electric powertrain efficiency was determined. After discovering the thermal effects on the inverters IGBT and the diodes power output, we now have a ball park idea of how efficient the vehicle will be in a drive cycle, at approximately 60 degrees Celsius, that does not produce consistent accelerations and decelerations. This analysis shows gives the team some idea of what to expect with regards to efficiency, but the simulation does not model a drive cycle common to the team driving tests.

Chapter 4. LV Optimization

As mentioned in the previous chapter, the electrical team set preparations and underwent an optimization phase. By year three of the competition the electrical portion of the vehicle appeared to be stable and functional with a few minor issues such as diagnostic trouble codes (DTC). Although these problems existed, they did not hinder functionality. Because there were no obvious complications, the team then had to extensively probe and analyze the vehicle to determine potential dormant issues.

To ensure that the electrical system continues to perform reliably meeting all requirements and to increase longevity, an optimization plan has been created. The auxiliary battery, the DC/DC converter, the power distribution unit, and controllers will be the primary devices under observation. Each component mentioned was added or can be affected by the teams added components, so must be analyzed. All data collected will be collected via an mBed controller. These devices also play critical roles in vehicle's operation. The goal of the optimization plan is to help the electrical team determine how well the electrical system is built.

The electrical team will use the manufacturer's given data to create a model that will simulate expected outputs. Information not provided by the manufacturer will be substituted for isolated bench test data, in which the component is isolated from all other devices and operated on its own. By doing this the team will at least know the best possible performance of the component during operation. This test is only as valid if the component is tested using the vehicle's intended power supply, which too must be isolated from all other loads including HV loads. The vehicle's stock components will be modeled based on the baseline data collected in Year 2 before any changes were made to the stock vehicle. The model data produced at that time will be used to compare with the empirical data. If the measured data is within 5% of the ideal model data, the electrical team will deem the system acceptable. Any measurements outside of this margin will

require more refinement and observation based on the differences and component itself. With regards to the ripple voltage, the electrical team will determine if the noise produced is significant for an added component and develop a method to compensate for such noise. Based on the EMI data, the team can move the communication buses away from areas of high intensity to ensure optimal data transfer or implement EMI reduction methods such as a faraday cage for example.

4.1 LV Ideal Simulation

To determine the current state of the electrical system a simulation of the entire vehicle's 12v system was done. This model would represent the ideal or minimum acceptable state of the LV electrical system. The ideal model is designed to be compared with the system implemented to determine abnormalities of the mule vehicle electrical system. Each added component was modeled based on the manufacturer's data or an isolated bench test. The stock components were modeled based on the vehicles baseline evaluation, because General Motors does not provide enough information regarding their components and circuits. Besides that fact, the stock system is exceptionally large and would require a great deal of effort to simulate correctly. The baseline evaluation consisted of collecting data on the 12v system of the vehicle prior to adding or removing any of the stock components. The data collected consisted strictly of the current draw of the entire system in accessory mode, sleep mode, and while the engine was running in park. No data was collected while the vehicle was moving.

Figure 32 shows the overall model of the electrical system. As mentioned before the Stock components are modeled, accessory mode, parasitic loads (included in accessory), and the engine running in park. In this model the new LEA and fuel driver expected to draw roughly the same amount of current as the LFX ECM and fuel driver along with similar behaviors. Each subsystem is given 12v battery voltage along with a signal that signifies that the vehicle wants to be turned on.

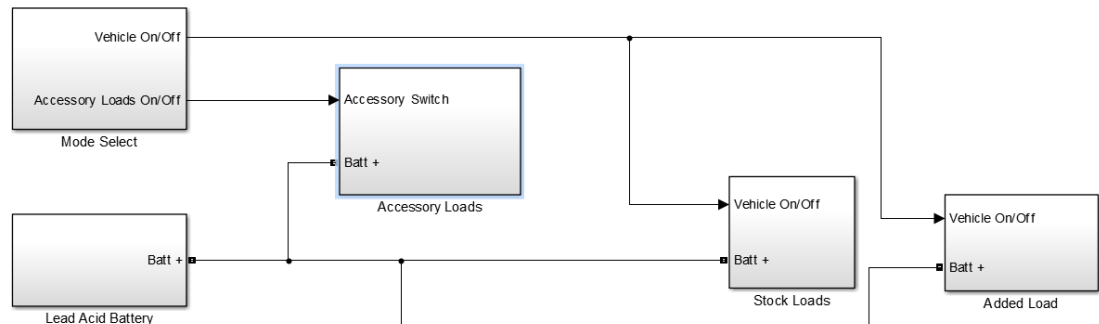


Figure 32: Overall Model

The accessory loads are modelled around the accessory loads measured within the vehicle while the vehicle was still stock. Figure B 3 gives the data collected for such loads. Every component and switch was used to produce the waveform that was depicted from the stock vehicle data. A timer is used to reduce the initial load if accessory or vehicle “on/off” signal is not present, forcing the subsystem to enter a sleep mode. This would reduce the vehicle current to roughly 12 mA. (Update Block below)

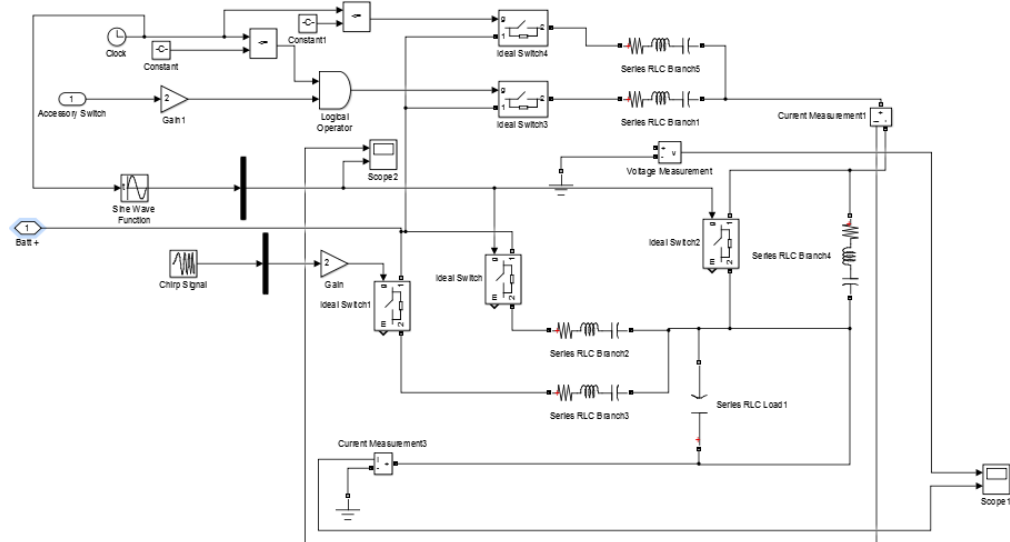


Figure 33: Accessory Load Model

Much like the accessory loads, the engine loads were modeled based on the baseline evaluation of the stock vehicle. The engine model is given in Figure 34. Figure B 1 in the appendix shows the current draw while the engine is running right after start up or run crank. The current decreases over a period of thirty approximately seconds, and again shortly after. The steady state current turns out to be about 18-20 amperes. Timers were used to model this unclear behavior.

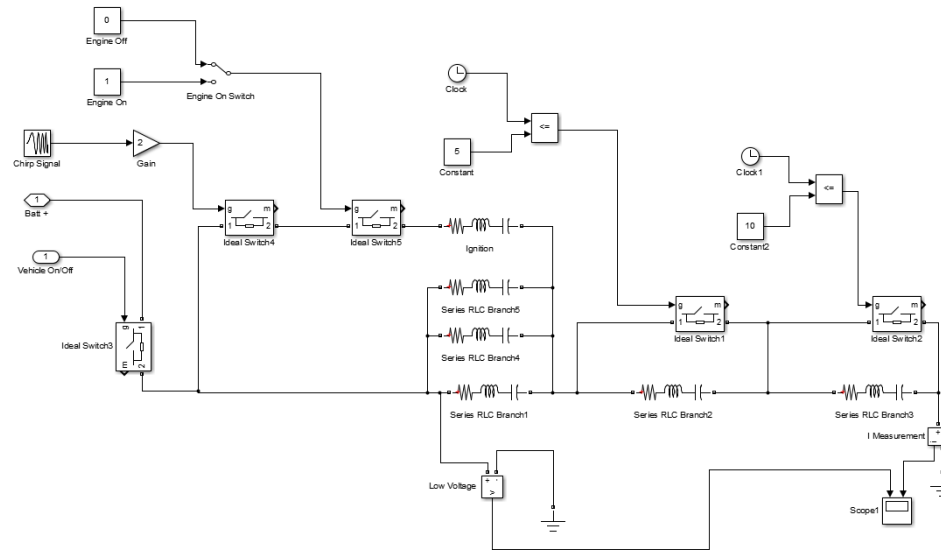


Figure 34: Engine Loads

The added loads subsystem is the primary subsystem under analysis. There are eight relevant loads within the vehicle, namely the MircoAutoBox, the HV electrical power modules cooling pump, the engine/radiator fans, the BMS, the inverter LV system, and the two clutch actuators. Appendix A 2 portrays the subsystem for the added controller. Each load is triggered by the vehicle on signal. After evaluating the vehicle mode of operation, it was determined that essentially all loads turn on in all vehicle modes of driving operation. The driving operation modes are charge sustain (CS) mode, charge deplete (CD) mode and sports mode. CD mode is a mode that uses only the engine to propel the vehicle while maintaining the 12v system. In order to enter this mode, the HV system must be utilized to start the engine, as a result all added components are used to some extent except the inverter's cooling pump. CD mode uses all the added components except the radiator fans. This

mode utilizes only the HV ESS to propel the vehicle. The fuel driver can also be discounted in this model seen that it draws a substantial portion of the overall vehicle loads. Both CD Sports mode uses all the added components except the radiator fans which is used in CS mode.

4.2 LV Vehicle Measurements

A great deal of vehicle testing was done to allow the electrical team to validate the electrical system. Several of the electrical behaviors are not ideal and there may exist quiescent issues. Although the electrical system was validated, verification is still essential in designing a vehicle capable of going 3000 miles without any major malfunctions. By verifying the electrical system, the team will determine if the system is built to the requirements and the power draws are comparable to manufacturer specifications. To verify the LV system, we will need the list of equipment seen below. Table 1 gives the various equipment needed, their availability, what it will interface with, and the vehicle condition while collecting data that will be used for optimization.

The multi-meter will mainly to aid in the troubleshooting of various sub-systems on the vehicle, but the readings will also be used to validate that the other methods of data acquisition are yielding correct results. This will give confidence that our other data readings are accurate. To collect instantaneous and time varying current and voltage data, an Mbed LPC1768 will be used to record the values which will then be uploaded to a computer for further analysis. The oscilloscope will be used for high frequency measurements such AC ripple. The EMI meter will be used for measuring the EMI from the electric motors within the engine bay. A voltage diver circuit will be used to measure the voltage on the various components listed later on and also for the system as a whole.

Equipment	Availability	Interface	Vehicle Condition
Multi-meter	Available	Battery	Vehicle Parked
		Fuse box	
		PDU	

Oscilloscope	Available	DC/DC Chassis ground	Vehicle parked & All modes on dynamometer
Current Clamp	Available	Battery Fuse box PDU	Vehicle Parked
Hall Effect	Not Available Must buy	DC/DC converter Aux battery	All vehicle modes
Shunt	Available	Aux Battery DC/DC converter	All vehicle modes
A/D Logger	Available	Shunt & hall effect sensor	All vehicle modes
Voltage Divider	Fabrication	Aux battery DC/DC converter	All vehicle modes
EMI Meter	Not Available	IMG motors, & inverters	All modes on dynamometer

Table 1: Measurement Equipment Used

4.3 LV Comparison & Analysis

Each component simulated will be compared to the empirical data. Acceptable criteria will be determined based on the manufacturer data and expected outputs/inputs based on research studies. For better analysis, the time frame of the simulation was skewed to overlap the vehicle data. The vehicle data is expected to be much noisier than the actual simulation due to non-ideal instrumentation.

4.4 LV Mitigation

The issues found after running simulations and collecting data are addressed at the end of each comparison and analysis section. Each problem is mitigated or a plan is given on how to mitigate the issue. The solution to the issues are based on the manufacturer's data, or a standard given by a company or industry. A 20% error margin is given to account for simulation error and vehicle abnormalities, such as axillary battery deterioration. Some of the mitigations failed on the first

attempt, and thus a second mitigation plan would have been conducted for different components. Finally, some components revealed multiple issues or potential issues after researching and solving a problem.

4.5 Aux Battery

The electrical team observed voltage drops, current spikes and parasitic draws on the 12v, 70 Ah, lead acid auxiliary battery. A shunt, a Hall Effect sensor, and a voltage divider circuit will be used to accomplish these tasks. Although the aux battery is not an added component it is still greatly affected by team added components. The methods given below will allow the electrical team to view the system as a whole and not at the component level.

The shunt was inserted into the main positive line at the aux battery and terminated using lugs with an mBed controller to measure the voltage drop across the resistor. This will be a temporary setup to measure the parasitic current draw during vehicle sleep mode. The Hall Effect sensor will be inserted anywhere along the battery's positive line to measure current transients and time-varying currents. To measure voltage spikes and drops of the battery, a voltage divider circuit will be fabricated on a breakout board.

An analysis was also done on the 12v charging of the battery using the data collected from the Hall Effect sensor. To avoid over powering the aux battery, calculations are made based on the manufacturer's data to determine maximum current draw of the unit, how long the maximum current can be drawn and the long term charging current.

The parasitic draws were measured while the vehicle is off or in sleep mode. All other measurements will be taken during every vehicle mode.

4.5.1 Aux Battery Simulations

Simscape provides a battery block that simulates a lead acid battery. If the block is given the right parameters, the battery behaves like a real-world battery. The voltage is reported, the SOC, and the current draw. With this, the 12v system can be even more accurately modeled. See Figure 35 for the 12v battery model subsystem. The 12v battery does not play a major role in the simulations, because accessory mode and parasitic loads weren't the teams concerns. There is a 12v disconnect switch that can eliminate parasitic draw problems, and accessory mode is rarely used. Although, the electrical team used this simulation to prove that the vehicle's parasitic draws were low enough to leave the vehicle down for approximately 30 days without fully depleting the 12v battery. What is most important about the battery block is that it can yield charging currents from the DC/DC converter.

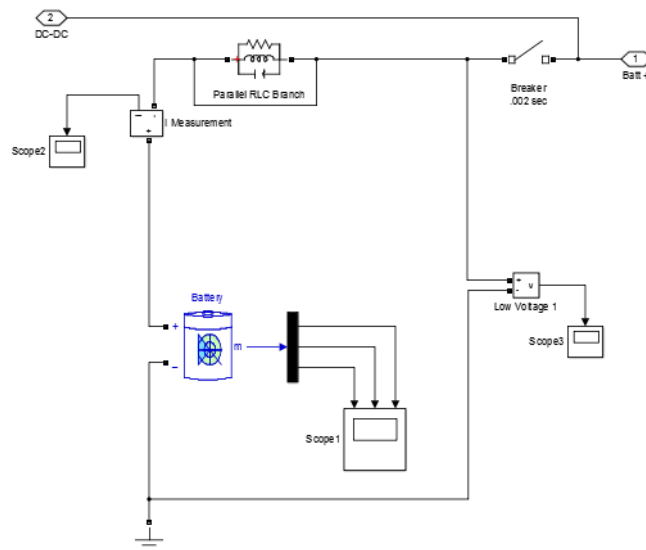


Figure 35: Lead Acid Battery Model

4.5.2 Aux Battery Vehicle Measurements

Using a voltage divider circuit, the 12v battery voltage has been captured for 15 seconds. The measurement was taken directly across the lead acid battery terminals. This data was sampled at 1 millisecond intervals or 1000 Hz. The data shows the voltage dropping from 12.9 volts to 11.2 volts

for 4 mille-seconds. This significant drop is assumed to be due to the initial transient current surge. From there the voltage rises to roughly 12.7 volts and eventually starts to drop to 12.5 volts. The transient behavior is the primary purpose of this measurement. The 12v lead acid battery is expected to initiate between 13 volts-12.6 volts, then steadily decrease over time with more of a decrease occurring during the earlier timeframe due to loads not entering sleep mode. The voltage becomes more stable after about 10 seconds after the vehicle has been turned on. This is due to the vehicle's components drawing less current in sleep mode.

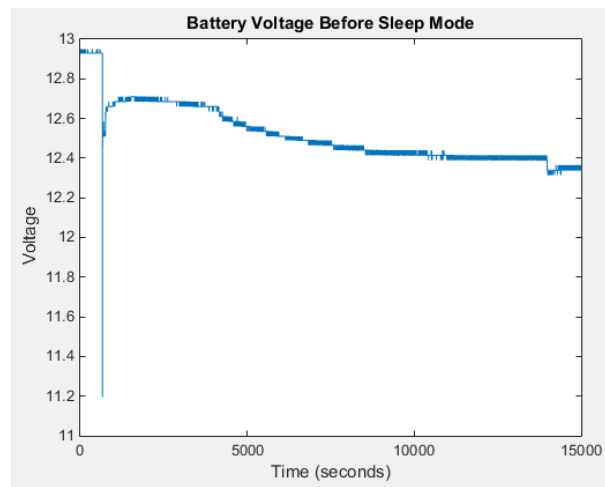


Figure 36: Battery Initial Startup Voltage

Figure 37 shows the 12v battery initial current after the main vehicle's 12v disconnection switch was closed. When the switch is closed there is a transient spike about 27 amps for a millisecond. The current quickly drops to less than 5 amps. As the vehicle continue to power up the current increases to an average of 8amps for a little over ten seconds. The vehicle then begins to enter a sleep mode by consistently reducing the current from roughly 3 amps – 900 milliamps. After another five minutes, the vehicle fully enter sleep mode.

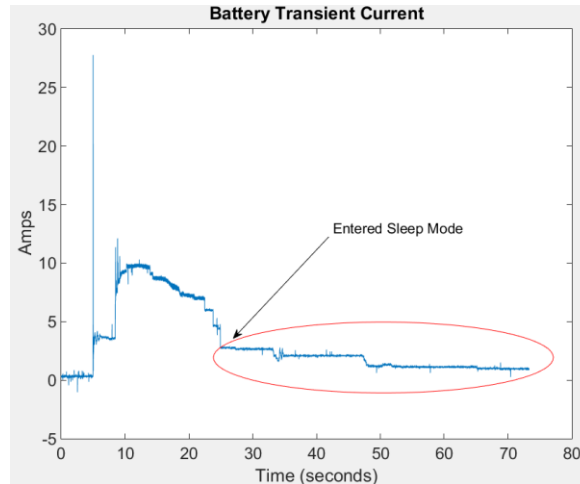


Figure 37: Battery Initial Startup Current

After measuring the battery voltages and currents when the 12v switch was initially closed, readings were then taken in charge deplete and with the engine on. Figure 38 shows the battery voltage while the vehicle was in park. Initially the voltage starts out as charge deplete responses, then after thirty seconds the engine is turned on. The decrease in voltage from 14.3v – 13.8 v occurs due to the high beam lights being turned off. A control strategy exists to ramp up the DC-DC voltage for better head light illumination. When the engine turns on, the DC signal has a 100mV fluctuation.

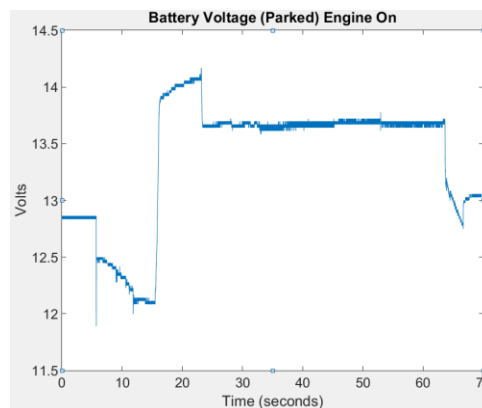


Figure 38: Battery Voltage (Parked) Engine On

The 12v battery current behaves in an expected manner. Figure 39 shows the behavior. Before the vehicle is turned on it supplies the vehicle with power and immediately when the vehicle turns on

current is being supplied to it. The current starts out as 20 amps and decreases steadily to 6 amps of charging current. Over time the current is expected to reach approximately zero amps. Just as with the voltage the current signal becomes noisier when the engine turns on at 28 seconds of measuring the voltage. After a minute the vehicle is turned off, so the 12v battery begins to charge the battery.

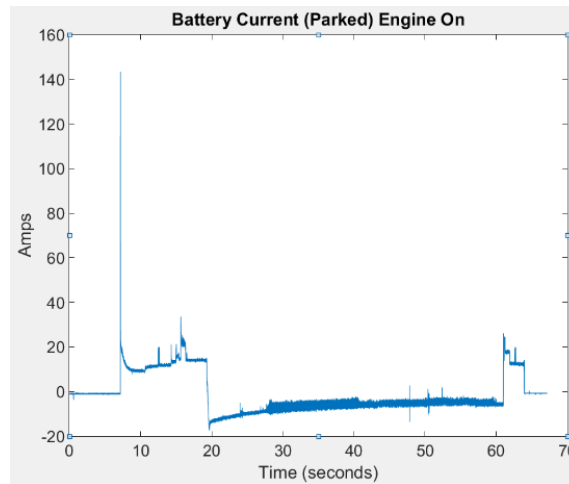


Figure 39: Battery Current (Parked) Engine On

4.5.3 Aux Battery Simulations & Comparison

Figure 40 depicts the auxiliary battery voltage when switching the vehicle's 12V disconnect switch on. In both cases the vehicle goes to sleep and reaches a steady state voltage. The initial voltage drop is much more intensive from the vehicle. This is expected because the battery's state of charge within the vehicle was not at 100%, whereas the within the simulation the SOC was at 100%. The vehicle's battery is also a year old and has been fully discharged to zero volts once. The initial voltage drop is more severe within the data because the current spike is more severe compared to the simulation. As seen in Figure 41 the current spikes to roughly 27.5 amps during initial startup, whereas the current only spikes to 15.5 amps within the simulation. The most crucial part of the two measurements lies within the transient spike which is on the order of at least 1 KHz. Because

the voltage sags and not spikes it is not an issue worth noting. The voltage also only sags to 11.2V, which is within the operating voltage range of every component within the vehicle.

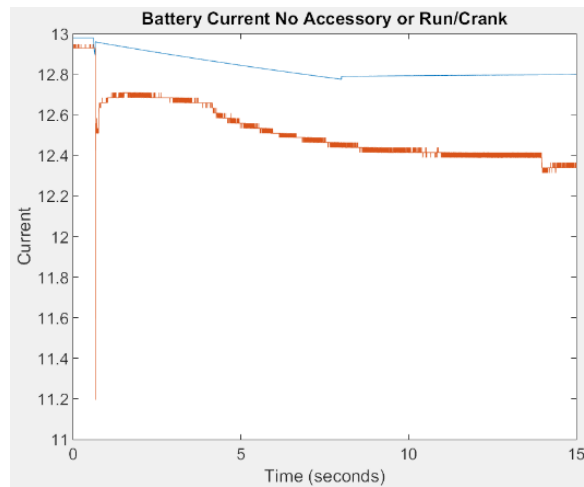


Figure 40: Battery Voltage with no accessory of Run/Crank

The transient current spike is the current drawn from the 12V battery. The linearly decreases the current from 8.5 amps to 8 amps and the vehicle went into sleep mode which is roughly 0.125 amps. The vehicle sleep mode current is higher, but the Hall Effect sensor loses sensitivity at roughly 2 amps based on experiment. The vehicle baseline evaluation shows the vehicle drawing 3 amps in accessory mode for 20 seconds, which is seen initially. It is assumed then that the added components turned on several seconds later. The simulation assumed 8 amps would be drawn steadily and instantly, hence for the difference in the two graphs.

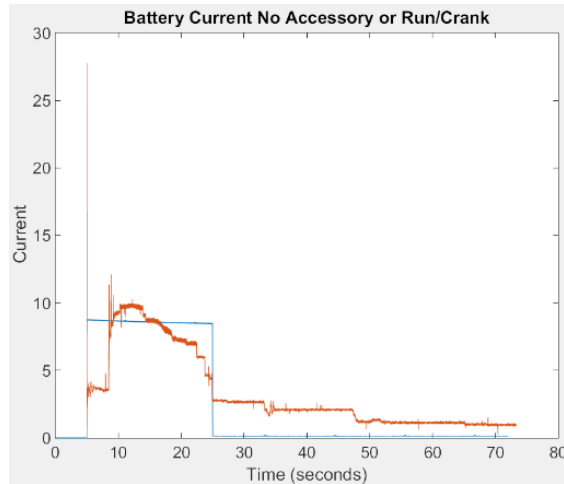


Figure 41: Battery Current with no accessory or Run/Crank

Next, a comparison is done on the aux battery component. The battery essentially is always being charged while the vehicle is on. The initial current spike is due to inrush/transient's currents spikes. The spike duration is less than 200ms, is acceptable seen that the discharge current is over 300 amps for turning an engine over in the stock vehicle, see B 4 in appendix B. The simulation does not produce any transients as seen in Figure 42 initially. This is primarily due to the filtering circuit used within the DC-DC converter.

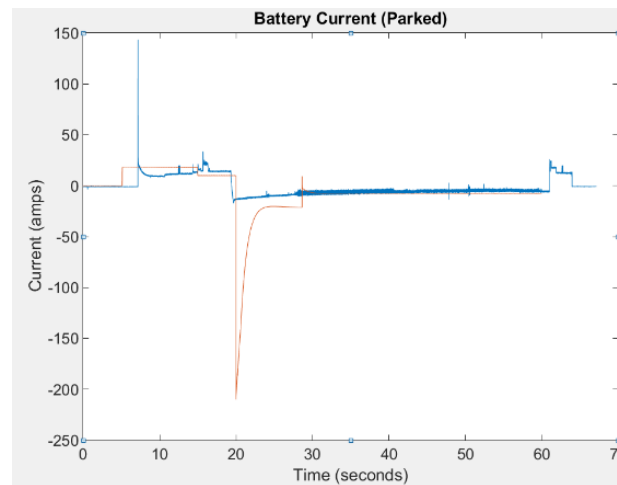


Figure 42: Battery Current (Parked) Engine On

The battery voltage as seen in *Figure 50* yields the battery's voltage before the DC-DC converter turns on and after it turns off. The simulation data follows a similar pattern, but it is still slightly

different. The actual battery's voltage drop considerably when initially turned on. As mentioned before in the previous sections, the actual 12v battery has some wear and so it is expected to behave with less performance. The simulation does however, lag when trying reach its peak voltage of 14.1v. The engine noise produce was also negligible in the simulation, whereas the actual vehicle battery portrays obvious noise when the engine turns on. The two systems behave relatively identical towards the end.

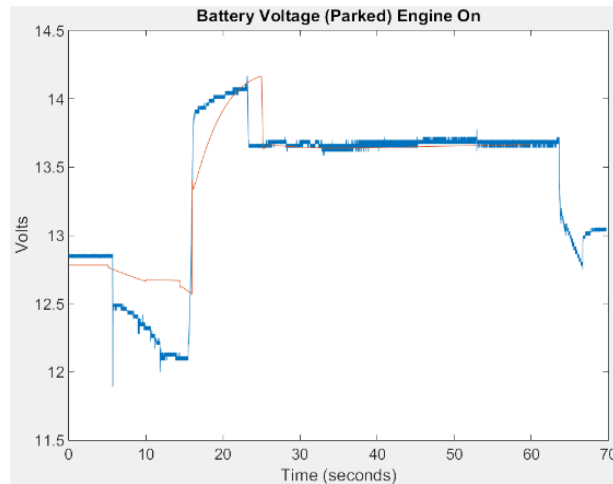


Figure 43: Battery Voltage (Parked) Engine on Comparison

4.5.4 Aux Battery Mitigations

The 12v auxiliary battery is sensitive to high voltages, high currents and ac ripple voltage and currents. Based on the measured and simulated DC-DC converter output, high voltage is not a problem. Overcharging the battery however is very simple to do. Once the 12V battery reaches a certain threshold voltage the internal resistance decreases, allowing overly high currents to pass through. An experiment was done to determine if a control strategy exist to avoid damaging the battery from overcharging. For the experiment, the 12V battery was simply discharged to approximately 12V or less. Then turning the DC-DC converter on. A staggering current transient of over 300 amps was drawn from the DC-DC converter for a moment in time, see Figure 44. Even worse the DC-DC converter charged the 12V battery at roughly forty amps for an excessive amount

of time. The auxiliary battery was measured at about 12.0 volts before turning the vehicle on. To compensate for this dilemma, a control strategy was implemented to avoid high currents from flowing through the battery.

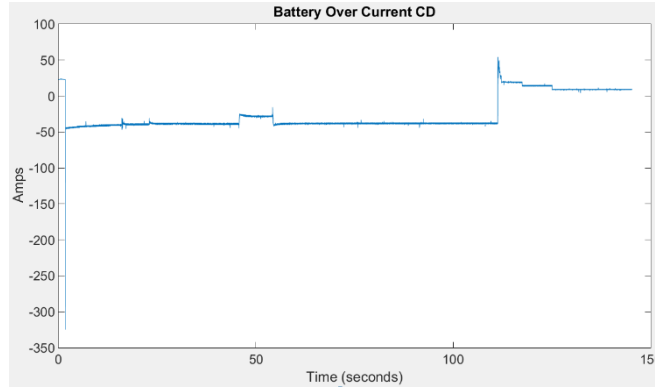


Figure 44: Battery over Current Charge Deplete Mode

The amount current and capacity of a lead acid battery depends on the amp hour (Ah) of the battery, see appendix E 2. The vehicle's battery's Ah capacity is 70 Ah. This number can be used to calculate the amount of current allowed during bulk charging. Using the 70 Ah number to calculate the current is given by,

$$I_{20} = > C_{20} = 70 \text{ Ah}$$

Where C_{20} is 20-hour capacity and I_{20} is the current discharge or 20-hour capacity,

$$I_{20} = \frac{70 \text{ Ah}}{20}$$

$$I_{20} = 3.5 \cdot 10 \text{ A}$$

$$= 35 \text{ amps}$$

To compensate for the access current drawn by the auxiliary battery the DC-DC converter voltage can be decreased from 14.3v to a lower voltage depending on the current drawn by the battery. A Hall Effect sensor will be used to determine the current flowing through the 12v battery. If the

current flow exceeds 35A for more than ten seconds, then the voltage will be dropped until the current is reported less than 35 amps.

4.6 DC/DC Converter

This component was observed similarly to the aux battery, where the team measured time-varying current draws and spikes. Voltages was also measured using a voltage divider circuit. Parasitic draws, however, will not be measured on this component. The measurements taken can be used to observe to view the overall system behavior.

A Hall Effect sensor was used to measure current spikes along with the time varying currents. This sensor was inserted on the positive line of the DC/DC converter. A voltage divider circuit was tapped off of the main output terminal to measure the voltage drop. A voltmeter and a current clamp was used to justify measured results are within a predicted range.

These measurements was conducted on every operational mode of the vehicle, except when using the voltmeter and the current clamp. Because the volt meter and current clamp are used for references they were only used when the vehicle was in parked.

4.6.1 DC-DC Converter Simulations

The DC-DC converter simulations were created based on the manufacturers. Not all information was given, such as how the converter itself compensates for load changes, transitions between the aux battery and voltages request changes. For the voltage changes segment, a simple bleed off resistor was used to simulate the vehicles' headlights being on. This resistor was also used for the transitions between being off and on. The model is given below in Figure 45. This model was modified from the HV optimization section to accommodate the dynamic behavior of the low voltage system.

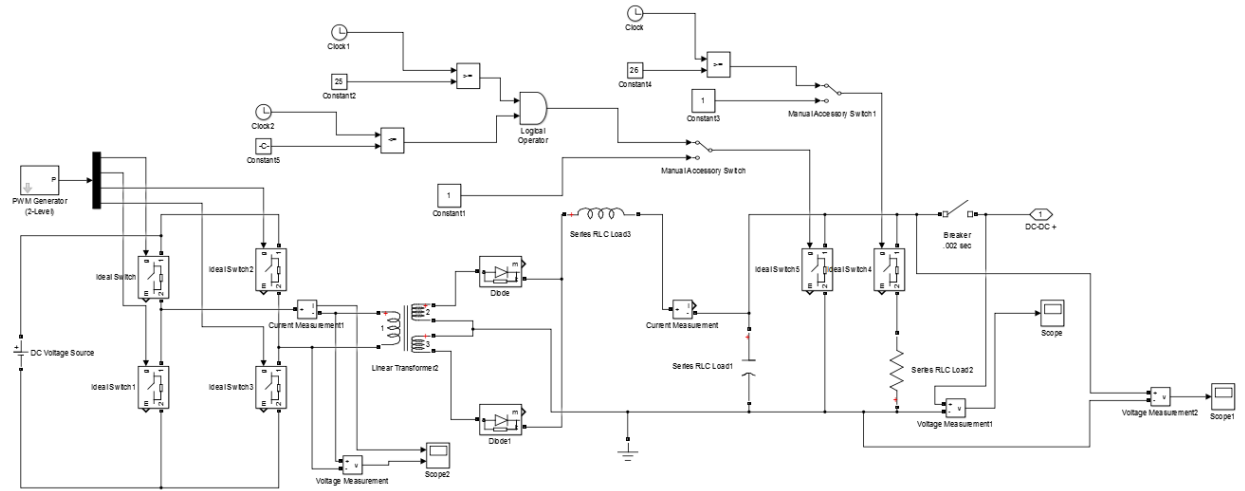


Figure 45: DC-DC Model

4.6.2 DC-DC Converter Vehicle Measurements

The DC-DC converter voltage was measured using a voltage divider circuit, as all the other voltage readings. When the vehicle is turned on at approximately 25 seconds the voltage on the DC-DC main leads rise to 14.3 volts. The head lights were left on during this test for the entire duration of the measurement. After 35 seconds of measuring voltage the engine was turned on and the vehicle was left in park. The engine creates some noise, but does not change the amplitude of the voltage at any point any time. Figure 46 depicts these readings.

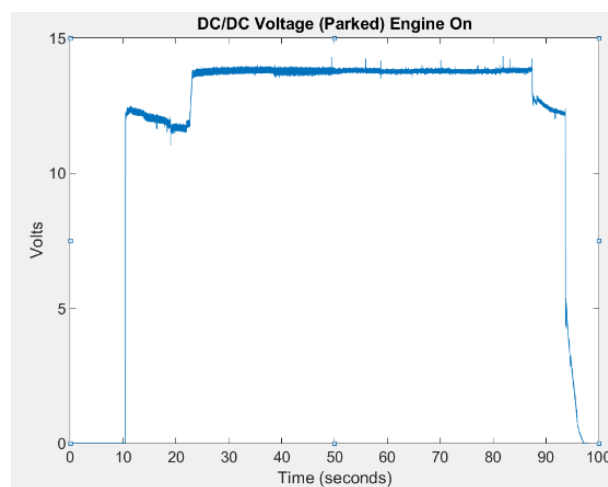


Figure 46: DC/DC Voltage (Parked) Engine On

Figure 47 displays the current measured on the DC-Dc converter main positive lead. The current spikes up to over 40 amps. At this point, there is no initial loads to be started because of the 12v battery being on before initiating the DC-DC converter to output power. The initial current drop is due to the 12v battery being charged up. And the current rises again by 5 amps because the engine was turned on. The steady decrease in current is expected to be due to the 12v battery charging. And as seen before the engine produces noisier signals than the fully electric mode. The drastic current drop at time equal about 80 seconds is due the head light being turned off. With this it is safe to say the headlight draw roughly 10 amps of current. The other blimps is largely due to the break booster being turned off and on.

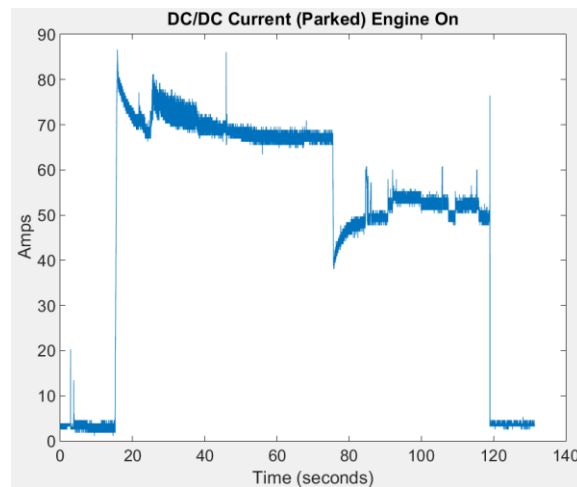


Figure 47: DC/DC Current (Parked) Engine On

Figure 48 shows the DC/DC converter voltage. This measurement was taken to verify the voltage bus behavior during charge deplete mode. The 12v bus climbs up to 14.3 volts in a manner of 500 milliseconds. There appears to be an initial voltage drop of approximately 100mV. The voltage sag occurring at the 72 second mark is due to the break booster being turned on and off for no more than two seconds due to stepping on the brake pedal. The other voltage drops occurring in the future is due to the vehicle's headlights being turned off and on.

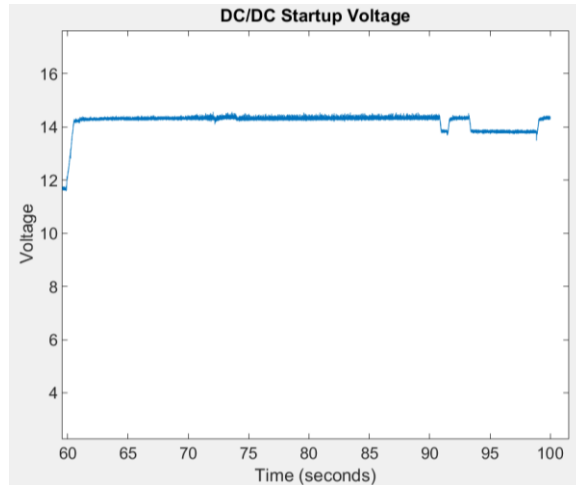


Figure 48: DC/DC Converter Initial Startup Voltage

4.6.3 DC-DC Converter Simulations & Comparison

Given below in Figure 49 is it is easy to see that the simulation voltage follows the DC-DC actual voltage. Again, the Simulation voltage is less than the actual battery voltage, but negligible. In this comparison, the headlights are turned off, so that battery voltage is roughly 13.8v. The engine noise that shows up the actual DC-DC voltage plot does not show up within the simulation plot although the engine ignition pulses off at twenty times a second six amps.

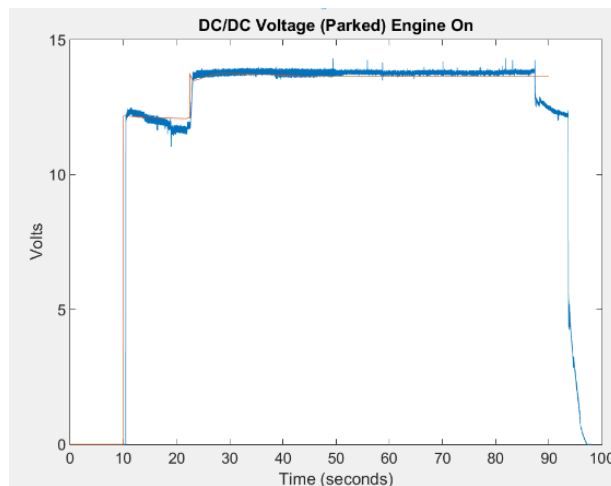


Figure 49: DC-DC Voltage (Parked) Engine On

Simulating the DC-DC current was more difficult than simulating the respective voltage. The battery dynamics along with the DC-Dc converter itself caused current transients to appear during

transitions. For example, when the DC-DC initially takes over the vehicle's loads the transient spikes easily rose above 300 amps. A bleed off resistor was added to compensate for such transients. In Figure 50, an unexpected sag took place twenty-two seconds into the simulated data log. Within the vehicle, the engine was turned on. In the simulation, the same task was performed, but the sag was much greater compared to the actual data.

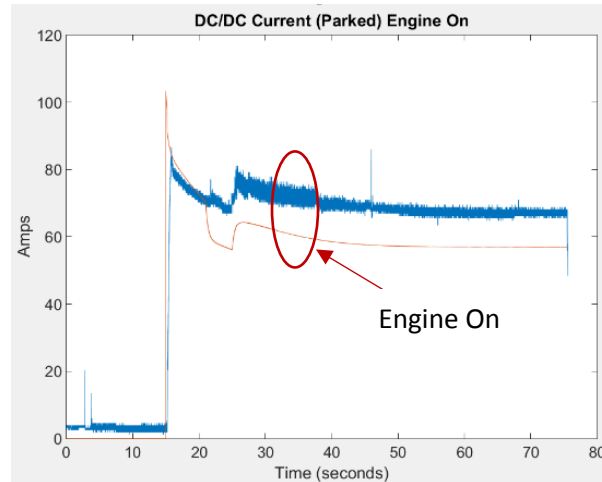


Figure 50: DC-DC Current (Parked) On)

4.6.4 DC-DC Converter Mitigations

The DC-DC converter operated correctly. The simulation itself, which is modelled to be ideal, is not as optimized as the actual DC-DC converter. Based on the analysis the DC-DC converter responds within seconds of current spikes and sags. The sample time is 1 kHz so the ripple voltage is not detected using the microcontroller.

4.7 Power Distribution Unit

The power distribution unit is an added component that powers the inverter and IMG electric motor coolant pump and the radiator fans. Instrumenting this component allowed the electrical team to analyze data on the component level. Voltages and current measurements were taken for each of the outputs using a Hall Effect sensor and a voltage divider circuit.

The voltage divider circuit allowed the electrical team to gather voltage drop data, while the Hall Effect sensor produce current draw over time and transient data. A voltmeter and a current clamp was also used as a reference for the measured voltages and currents.

This data was collected under all modes. As mentioned earlier the voltmeter will only be used while the vehicle is in park to verify the collected data is accurate.

4.7.1 Power Distribution Unit Simulations

Figure 51 shows the HV electrical cooling pump model. This pump controls the thermal characteristics of the inverters and the HV electric motors. The manufacturer data provided for this device was trivial, so this component was modeled based on an isolated bench test. Transient spikes were modeled; however, the motors steady state behavior was difficult to simulate. The motor is controlled by the power control module designed by the electrical team. The module pulses the motors at a duty cycle of 100 Hz using PWM signals. The radiator fans utilize the same subsystem with minor changes to the capacitance, inductance and resistance of the loads. The diode in the simulation was used placed in the simulation to determine the circuit behavior with and without the diode. With the diode in the circuit there was less negative voltage across the RLC load when the switch turned off.

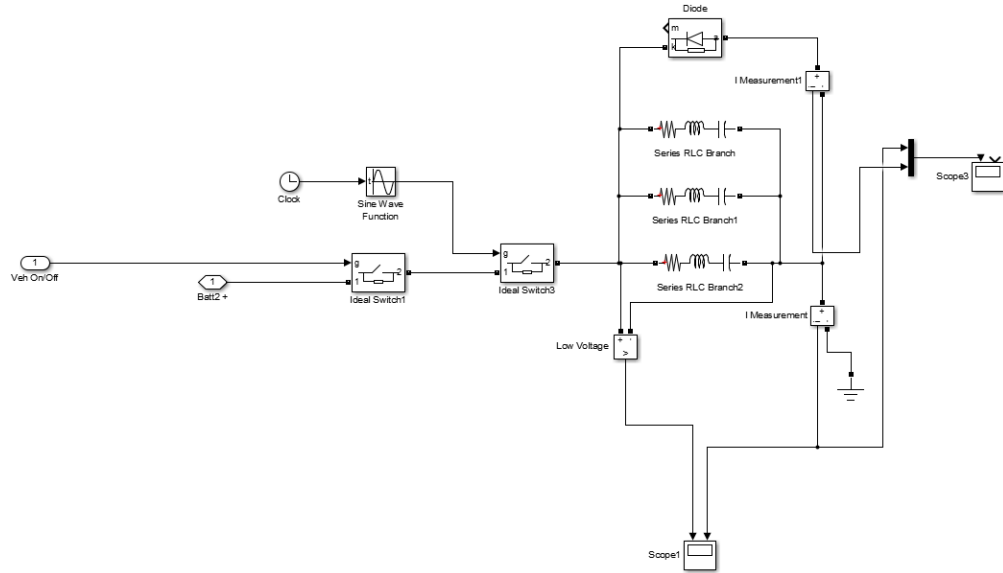


Figure 51: HV Electrical Cooling Pump Model

4.7.2 Power Distribution Unit Measurements

For the HV cooling system pump, only the voltages were read. Current readings were difficult to take due to the size of the wires and the placement of the harness. The Cooling system does not turn on unless the vehicle is on in charge deplete, charge sustain or engine only. The voltage measurements taken, Figure 52, shows the voltage rising to roughly 14.1V which means there is a voltage drop of 200 mV from the DC-DC converter to the output side of the power distribution module.

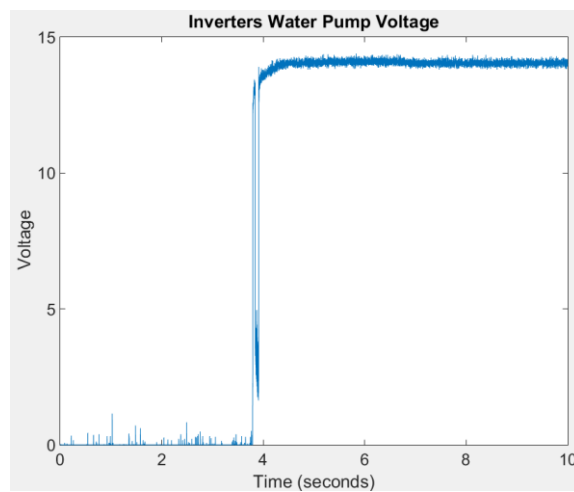


Figure 52: Electric motors water pump source voltage

Figure 53 shows the voltage sag across the HV cooling pump. The voltages drop to 2V, nearly 0V, for 50 milliseconds and eventually back up to 14V.

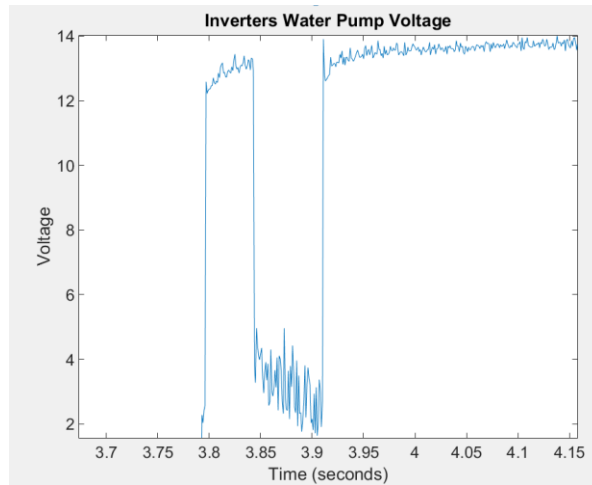


Figure 53: Zoom into power distribution module initial voltage

The gate of the cooling fan MOSFET was taken to determine the off and on behavior of the system, seen that pulse width modulation was an important aspect of the transistor. This reading was taken using an oscilloscope to view a more detailed behavior of the system with less errors due to noise. The PWM signal is 100 Hz with a peak voltage of 2.3V.

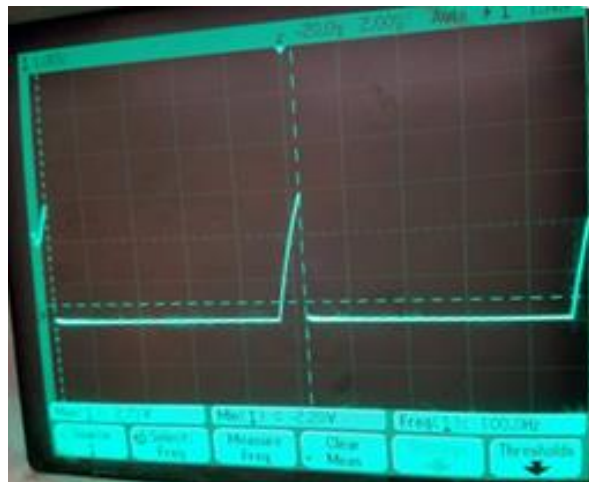


Figure 54: Gate of radiator fan MOSFET

4.7.4 Power Distribution Unit Mitigations

First the power distribution module was fixed using circuit analysis. Signal readings were taken at the microcontroller to ensure the right signals were being generated see Figure 55. Because the micro-controller yield the expected output, another measurement was taken at the bipolar junction transistor (BJT) that toggled the MOSFET's. The BJT's base lead was measured and the readings were portraying a 100 Hz signal, however it was not a square pulse and the amplitude of the signal was only 2.3V. See Figure 54 for details.



Figure 55: Mbed PWM signal output

Based on the signal of the base of the BJT, the signal was charging up and discharging. It was assumed that the signal needed more time to reach the source voltage, which is roughly 12-14V. With this assumption, the problem would then be related to the resistive and capacitive elements within the circuit, which is technically RC or time constant. Because the gate of the MOSFET is a fixed element the resistor was changed from a 100k Ω to a 1.2k Ω resistor. After replacing the resistors, the gate of the transistors now went fully on momentarily and fully off. The ripple or ringing affect was considered acceptable based on the fact that the fan's speed was capable of being varied.

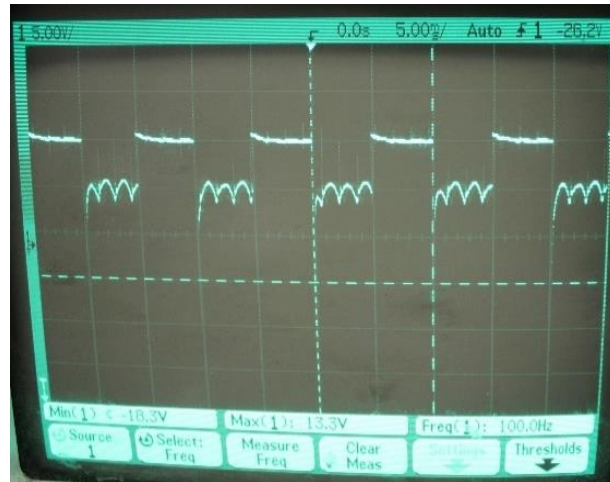


Figure 56: MOSFET Gate Voltage after Mitigation

The 12v drop that initially occurred across the motor was mitigated by adjusting the control strategy, such that the motors ramped up linearly, rather than instantly. By doing this the inductor would not require a large amount of current to start up, hence the voltage would not drop significantly.

4.8 Supervisory Controller

As mentioned before the supervisory controller is the primary controller within the vehicle and is used to control the hybrid powertrain and interconnect the transmission, the ICE and the electrical powertrain. The supervisory controller is a dSpace product called the “MicroAutoBox II” designed for rapid control prototyping applications such as powertrain, electric drive control and aerospace applications. Analysis was done on this product because of the vehicle’s high level of dependability on this product.

4.8.1 Supervisory Controller Simulations

The MicroAutoBox is more crucial and expensive than any other low voltage device within the vehicle, so more care was taken to determine the characteristics of this component. It was modeled based on the limitations given by the manufacturer and by bench testing with a switching power

supply along with 12v lead acid battery. The data collected from these tests and the manufacturer was used to model the controller in Simscape, see Figure 57.

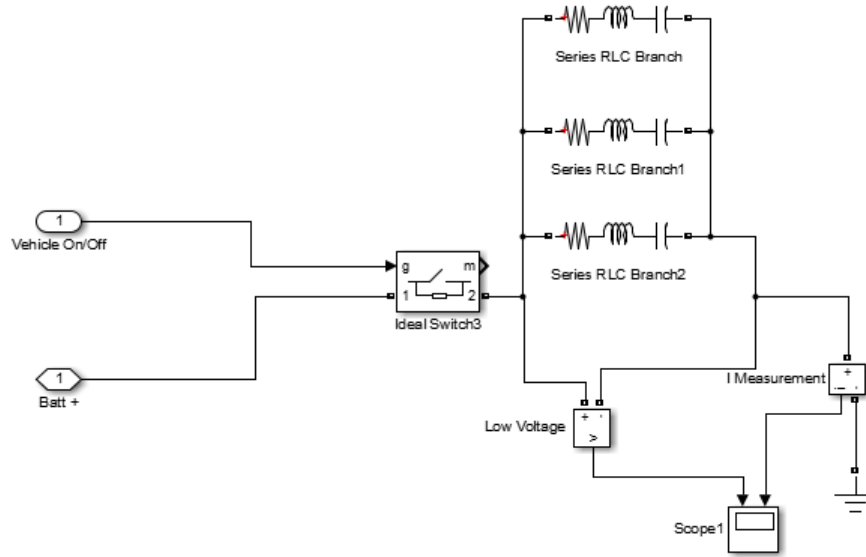


Figure 57: MicroAutoBox Model

4.8.2 Supervisory Controller Measurements

The supervisory controller voltage, as seen in Figure 58, has an initial voltage of approximately 13.1V with two sags of about 600mV - 900 mV. The sags both last for less than ten milliseconds. After the initial sags the voltage stabilizes and drops according to the 12V auxiliary battery.

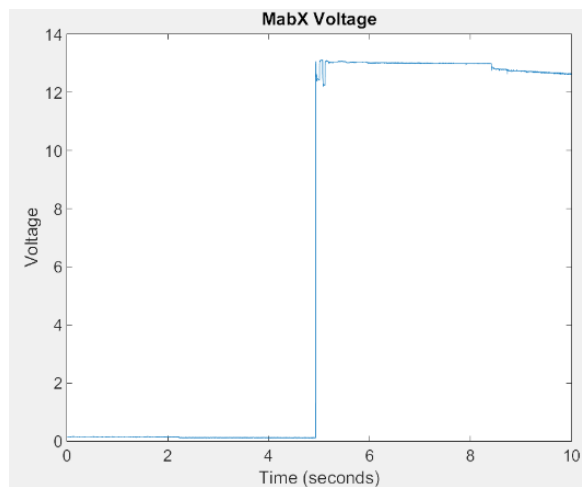


Figure 58: MicroAuto Box Initial Startup Voltage

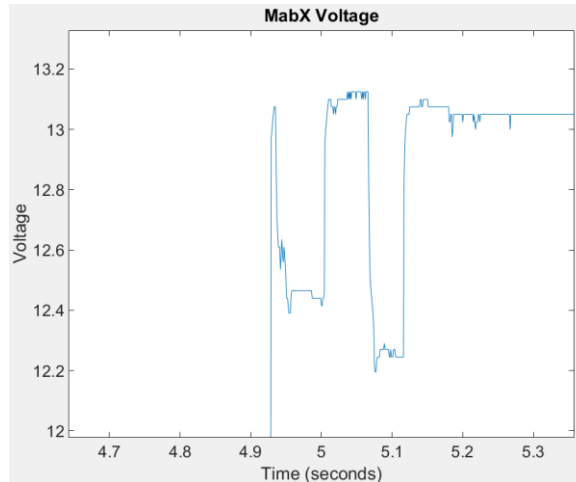


Figure 59: Voltage sag from Figure 59

The current drawn by the MicroAuto Box is at most 1.5 amps. It is stable and consistent from it reaches steady state. There is an initial transient greater than 2.5 amps, but overall the current is stable.

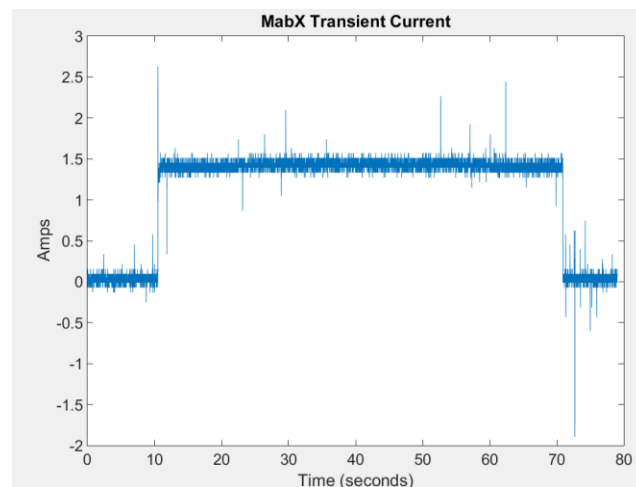


Figure 60: MicroAuto Box Initial Startup Current

4.8.3 Supervisory Controller Simulations & Comparison

The simulation and the empirical data is within 20% of each other. There is more of a voltage drop from the vehicle data initially, but this is due to lack of information from the manufacturer. The 12v battery also drops voltage faster than the ideal lead acid battery, which is probably to the fact that the actual battery has more wear and tear than the simulated battery.

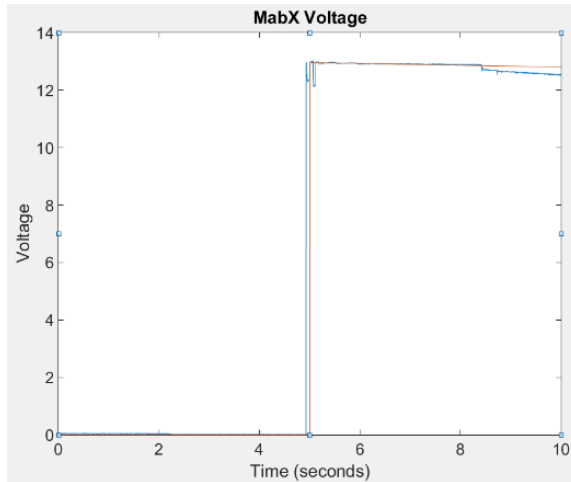


Figure 61: Supervisory Controller, simulation and empirical data Compared

The current from the supervisory controller was the component analyzed and compared to simulations. Figure 62 yields the current consumed by the MicroAuto Box. Based on the manufacturer data, the controller should not draw more than two amps continuously and no more than thirty-six watts. With this information, the model yields a 20% safety margin. In this case, the controller is consuming less current that is considered reasonable by the manufacturer. There is no concern with the data collected.

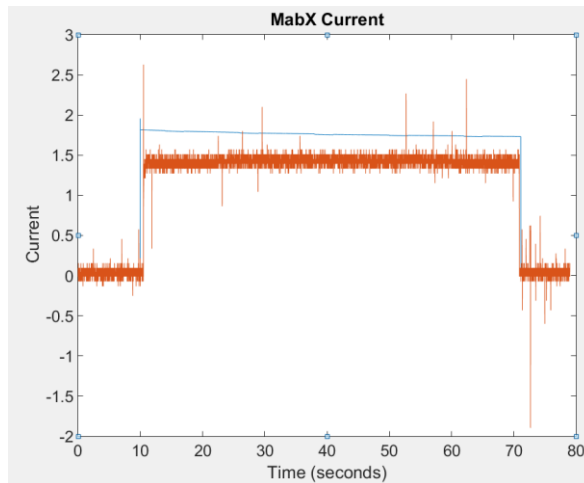


Figure 62: MabX Current simulated and measured overlap

4.8.4 Supervisory Controller Mitigations

The supervisory controller empirical data and the simulations are within the 20% margin of tolerance. Based on the data collected the voltage follows each other much closer than the current does. As with the other battery data collected, the axillary battery has been charged and discharged dozens of times, whereas the simulation simulates an ideal lead acid battery. Also, the transient spike lies within the maximum power output of the device which further indicates that the component's behavior is acceptable.

4.9 Voltage Ripple

Every LV component can be affected by a/c voltage ripple that may leak from the HV bus. Only an oscilloscope will be used to measure this data. To see full effect of the a/c ripple, measurements will be taken at the DC/DC converter output ports and metal/bonding frame to allow for a system overview. More measurements will be taken at the aux battery, the supervisory controller and various locations on the chassis ground to determine components level effects.

If the voltage ripple is difficult to capture, a current clamp which connects to the oscilloscope will be used to measure current ripples existing on the LV bus., particularly at the mentioned locations.

4.9.2 Voltage Ripple Measurements

The voltage ripple was captured on the 12v bus using an oscilloscope. Care was taken while probing the system, by ensuring no extensions were added to the probe leads. In doing so the team avoided creating an antenna which can produce noise from the environment yielding false readings. Although not shown in Figure 63 the frequency of the ripple was roughly 50 kHz with what appears to be modulated at sixteen-hertz. The voltage ripple has a peak to peak voltage of about 1.2 V peak-peak.



Figure 63: Voltage Ripple on 12v system before mitigation

The engine was not outputting maximum power after testing in the past. It was reported to loose approximately 40kW of power at wide open (100%) throttle. Figure 64 portrays the requested throttle versus actual throttle. The driver is requesting 100% power output from the engine, and the actual output is roughly 50%.

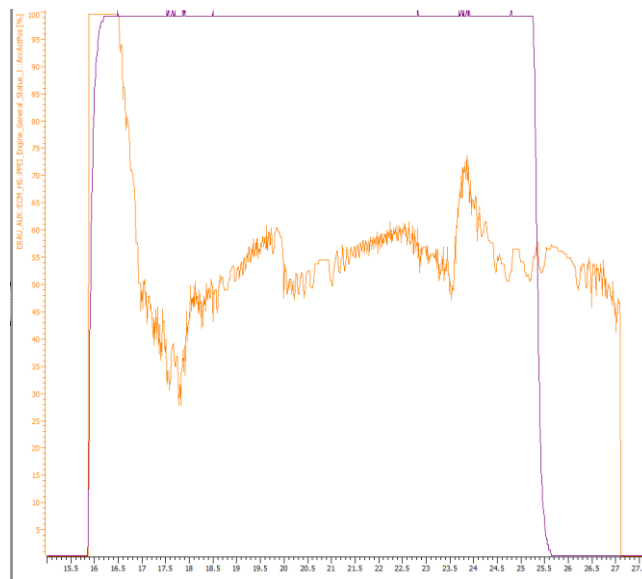


Figure 64: Requested Throttle vs Actual throttle

4.9.4 Voltage Ripple Mitigations

The voltage ripple was expected to be typically more than, given that manufacturer did not give information regarding the converter's ripple voltage. However, after rearranging the ground on the vehicle and taking another round of voltage readings, the 1.2 v 50 Hz waveforms reduced significantly to a voltage ripple of less than 800 mv peak-peak, see Figure 65. The ripple current and voltage also can play a key role in damaging the lead acid battery, so current reading were also taken to determine the bus ripple current. Figure 65 shows the current ripple as measurement two (2) in the window. The ripple voltages and current are negligible. Both measurements have a peak-peak output of less than 900mV.

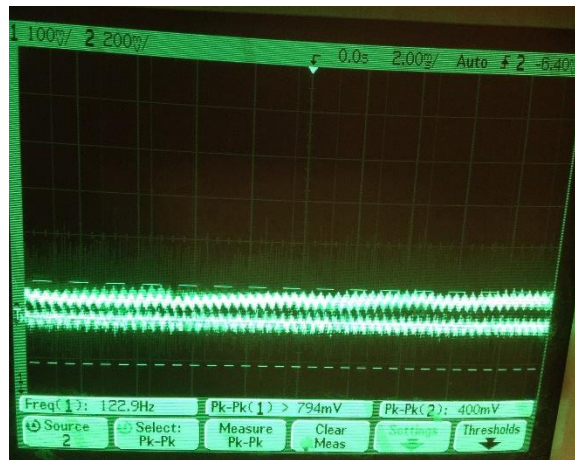


Figure 65: Ripple voltage and Current

With the rearranging of the grounds, appendix D 4 and D 5, the engines pedal noise was also removed. Figure 66 shows the new pedal output requested versus the actual pedal output. The color scheme of the output and requested were reversed from Figure 64 because the measurement was taken at different times, causing inconsistency.

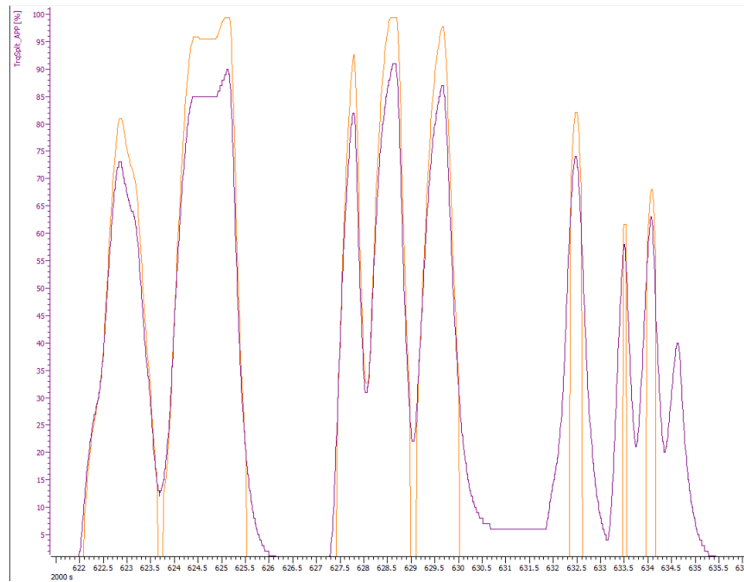


Figure 66: Mitigated Requested Pedal vs Actual Pedal

4.10 Additional Analysis

Electromagnetic Interference (EMI) and HVIL analysis were done, but not simulated due to difficulty and limitations of Matlab's Simscape capabilities. A ghost/EMI digital meter was used to determine the electromagnetic interference (EMI) emitting from the HV motors and inverters during dynamometer testing. This would allow the electrical team to view the effects from a system level and even at the component level with regards to EMI. Such measurement will not be logged but rather viewed and recoded.

4.10.1 EMI & HVIL Measurements

The Electromagnetic field interference was measured throughout the vehicle to determine areas of highest intensity. This information was used in deciding the CAN bus wire routing. By strategically placing the CAN bus throughout the vehicle, the optimal locations were used to yield the best results from the CAN bus. Figure 67 portrays the EMI at the HV distribution box. At this location, there is mainly DC lines on the input and output of the box from the HV battery. The meter shows 10.1mG of EMI.



Figure 67: EMI Reading Across the DC Lines

The image shown in Figure 68 shows the EMI measurement at the inverters from the HV distribution unit. This reading was expected to be higher than that from the HV distribution unit because the inverter itself switches off and on the voltage to create AC voltage. With an EMI reading of 85.5mG the inverter is roughly eight times higher than that of the HV distribution box.



Figure 68: DC Lines into the Inverter

As expected the three phase AC lines has a much high EMI that that of the inverter. The meter is limited to 200mG. The closer the meter is to the motor the more the meter reaches its maximum capability. Readings were consistently within the range of 185mG to “OL” over limit.



Figure 69: EMI Reading on Three Phase Cables to Motors

The HVIL issue was analyzed using a volt meter rather than logging the data because of the simplicity of the circuit. The HVIL circuit operates between a voltage range of 6-16V and a current draw less than 250mA. After troubleshooting the circuit due to a fault, a voltage drop of four plus volts was found from the drain to the source leads of the Metal Oxide Semiconductor Field Effect Transistor (MOSFET). Although the voltage drop is within the threshold of the circuit, the MOSFET operates inefficiently with this level of power loss.

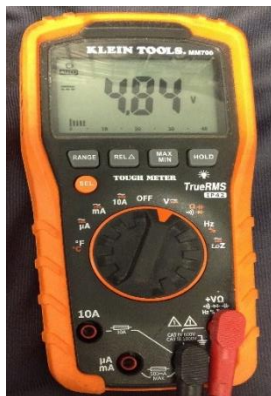


Figure 70: HVIL Voltage Drop

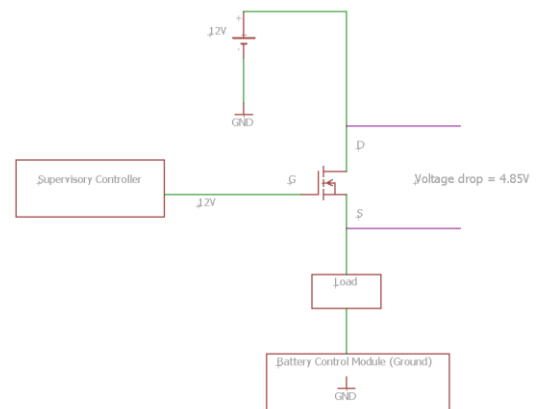


Figure 71: High Level Schematic for HVIL
Circuit

4.10.2 EMI & HVIL Research

Based on the research conducted during year one of the EcoCAR 3, it was determined that EMI less than 200 mG will not affect a CAN bus that is implemented correctly. Shielding is not required

so long as the wires are twisted pairs and routed away from EMI sources higher than roughly 120 mG. With proper shielding, it is suspected that a properly implemented CAN bus is immune to even the highest EMI the vehicle can produce. After bench testing on the Malibu and using high EMI sources such as solenoids, the created and tested CAN busses were unaffected with shielding.

After analyzing the HVIL circuit, and continuing research on MOSFET's, it was determined that the Gate-To-Source Voltage (V_{GS}) is directly related to the Drain-To-Source resistance (R_{DS}) [Using MSFETs in Load Switch Applications]. The greater the difference in potential between V_{GS} the less resistance between the Drain and Source of the transistor [Using MSFETs in Load Switch Applications]. In Figure 70 and Figure 71 the voltage drop is roughly 5V, which implies there is a large resistance relative to the load of the circuit causing voltage drop. With a current output on the circuit of less than 250mA, the transistor should appear virtually invisible. For the N-Channel MOSFET V_{GS} voltage to be large the source lead must be directly connected to ground, low side driver. Because the ground of the HVIL circuit is located within the BCM the transistor had to be changed to P-channel FET.

4.10.3 EMI & HVIL Mitigations

To ensure that the CAN bus is safe guarded from these intensities, each CAN bus was routed around or away from the electric motors and the three phase HV cables.

The HVIL circuit, which utilized an N-channel MOSFET, was replaced with a P-channel MOSFET. The supervisory controller now have to send a low signal rather than a high signal to turn the HVIL circuit on. As seen in Figure 73, this topology produces a V_{GS} that is now high enough to decrease the voltage drop to less than 10mV, Figure 72.



Figure 72: VDS of implemented P-channel MOSFET

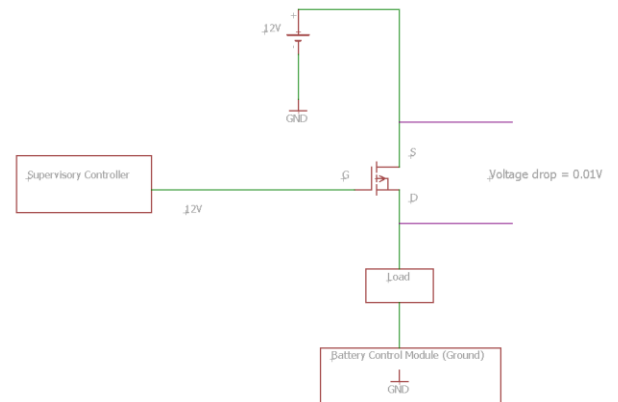


Figure 73: Schematic for new HVIL circuit

4.10.5 Parasitic Draw

The vehicle's parasitic current draw was reduced to 55mA. There was no data taken on the vehicle before the sleep mode circuit was implemented. However, the supervisory controller, GL200 (data logger) and the power distribution unit never went to sleep, so it is assumed that there was at least 3 amps of current draw consistently. *Figure 74* shows the current dropping from 3 amps to 2 amps, then to roughly 1 amp, and finally to 55mA. *Figure 75* shows a closer look at the final current drop during sleep mode. Due to the low current output during the final sleep mode current change, the data became very sensitive and as a result the current fluctuated between 90mA and 30mA. To prove the current draw was 55mA a voltmeter reading was taken between (series) the auxiliary battery main positive line and the battery positive terminal itself and given in Appendix D 6.

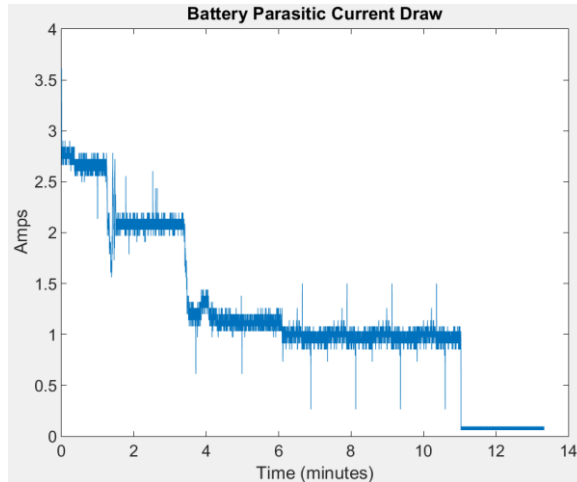


Figure 74: 12v Battery sleep mode Current

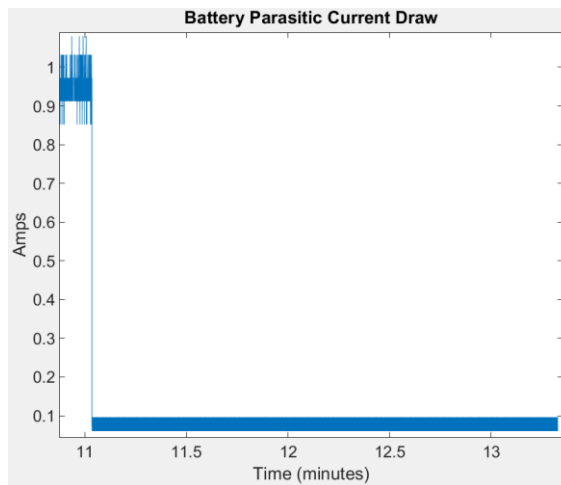


Figure 75: 12v Battery full sleep mode current draw

4.10.4 LV Conclusion

The low voltage system has been evaluated using simulations and empirical measurements to determine quiescent and prominent issues. Several problems were found concerning the power distribution module and voltage ripple, but they were all mitigated after researching. The significant voltage ripple was due to a ground loop within the engine bay, the accelerator pedal noise was also due to the ground loop within the vehicle. After separating the grounds, putting signal (sensitive) circuit grounds away from high current grounds, the apparent noise disappeared. The power distribution unit issues were solved as well via control strategy and replacing resistors to change

the RC time constant of the MOSFETs. The HVIL circuit was also corrected by replacing an N-channel MOSFET with a P-channel MOSFET. The vehicle's sleep mode current draw was also reduced to 73mA, which initially was roughly 3A.

Chapter 5. Conclusion

5.1 Conclusion

Research for EcoCAR 3 competition began the first year of the competition and continued throughout the years. CAN bus was studied to determine the electrical characteristics and limitations. A power distribution module was created to ensure that the team had a unit that could distribute high currents to devices throughout the vehicle. In the first half of year two of the competition, schematics were made, bench tests were conducted, along with a great deal of planning and coordinating. With the arrival of the vehicle, the foundation was set both theoretically and practically to begin and completely build the hybrid vehicle. A system engineering approach was taken to stay abreast of the overall team goals and keeping track of potential electrical issues that may have arose. This method proved to be affective given the drivability of the vehicle at the end of year three. During year three the team focused heavily on Optimization and simulations. Simulations were created for the HV electrical systems and the entire LV electrical system. These simulations were based on baseline evaluations from the stock vehicle and manufacturer data. The manufacturer data was especially needed to determine each components limitation and expected behavior. Data was collected from the vehicle and compared to simulations. In doing this greater insight was given on the vehicle from a component level and the overall system. The only severe transient spike found was current spike during the initial DC-DC startup, all other transients were within reason based the manufacturer data. The three problems presented in the paper were the power distribution modules inability to switch off and on, HVIL not receiving full voltage due and supplying to much current to the 12V battery. Overall the electrical system appeared stable apart from a few random current and voltage sags. No voltage spikes exist on any of the added components, more excessive current draws. The radiator fans and the HV motor pumps are the two prime factors for the voltage sags on the 12v bus.

5.2 Future Work

The vehicle is expected to outlast the duration of the four-year competition and longer. Collecting data can be a tedious process and can be time consuming. To alleviate this issue, linking all the data on the vehicle's CAN bus will make data acquisition much easier and convenient. Although, the vehicle's electrical system is expected to endure for several hundred to thousand miles, unexpected behavior may occur randomly, during unanticipated events or during rough drive cycles. Obtaining a deeper understanding of the electrical system can also be useful. A fault tree analysis can be helpful in determining issues before they occur based on data observation and deeper analysis. Finally, there exist many weak points within the vehicle that has proven to work for over several hundred miles with a high probability of not changing. As a result, solder joints can be replaced by crimps.

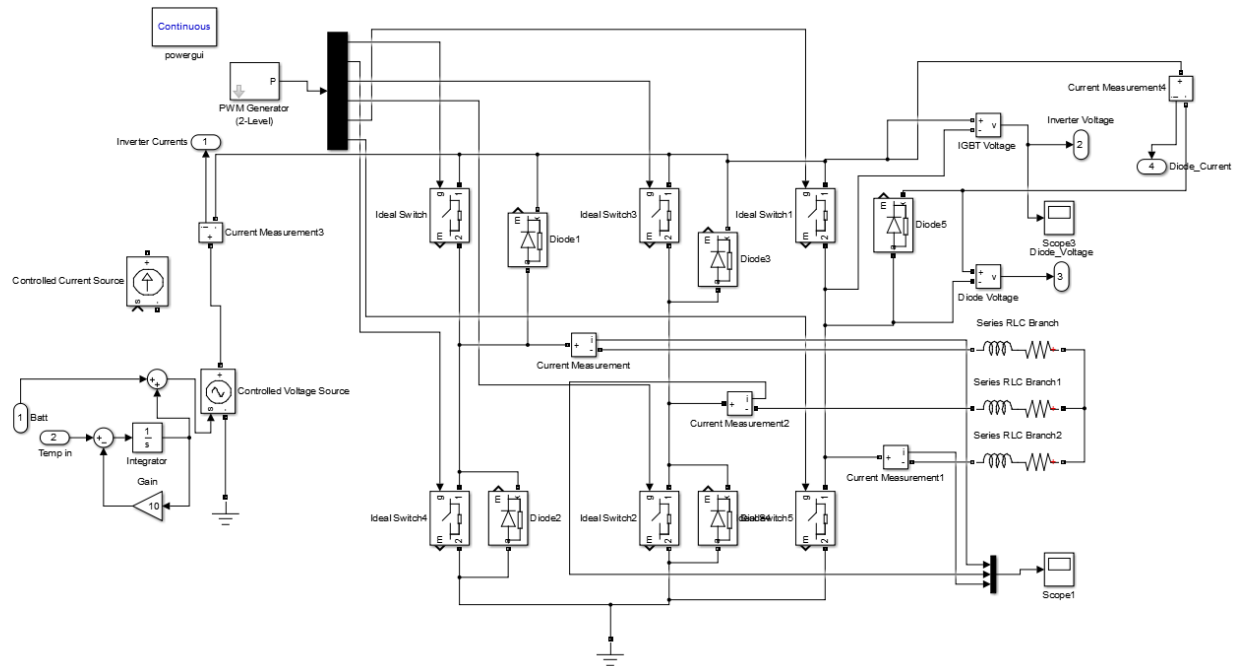
Chapter 6 References

- [1] "ecocar3," U.S Department of Energy , [Online]. Available: ecocar3.org/about/. [Accessed April 2017].
- [2] R. Atkinson, "Project Management: cost, time, and quality, two best guesses and a phenomenon, it's time to accept other success criteria," *International Journal of Project Management* , vol. 17, no. 6, p. 5, 1999.
- [3] E. Lechovic, B. Szewczykova, I. Kovarikova and K. Ulrich, "Solder Joint Reliability," *Materials Science and Technology*, no. 9, p. 8, 2009.
- [4] K. Kundert, "Power Supply Noise Reduction," *Designer's Guide Consulting*, no. 4, p. 12, 2004.
- [5] S. V. Vaseghi, "Noise and Distortion," in *Advanced Digital Signal Processing and Noise Reduction*, Chichester, John Wiley & Sons Ltd, 2000, p. 15.
- [6] J. Seymour, "The Seven Types of Power Problems," *Data Center Science Center*, no. 1, p. 21, 2001.
- [7] F. Silva and M. Aragon, "Electromagnetic Interference from Electric/Hybrid Vehicles," *General Assembly and Scientific Symposium* , p. 4, 2011.
- [8] B. E. Klipec, "Reducing Electrical Noise In Instrument Circuits," *IEEE*, Vols. IGA-3, no. 2, p. 8, 1967.
- [9] T. Williamson, "Designing Microcontroller Systems for Electrically Noisy Environments," *Application Note*, p. 26, December 1993.
- [10] G. Converter, "DC/DC Converter Output Ripple & Noise," Laval, 2004.
- [11] L. E. Fisher, "Proper Grounding Can Improve Reliability in Low-Voltage Systems," *IEEE*, Vols. IGA-5, no. 4, p. 6, 1969.
- [12] "Types of Applications of Measurement Instrumentation," p. 10.
- [13] R. Simpson, "Instrumentation, measurement techniques and analytical tools in power quality studies," *Pulp and Paper Industry Technical Conference*, p. 10, 2002.
- [14] R. A. Jackey, "A Simple, Effective Lead-Acid Battery Modeling Process for Electrical System Component Selection," MathWorks, Novi, 2007.
- [15] Z. M. Salameh, M. A. Casacca and W. A. Lynch, "A Mathematical Model for Lead-Acid Batteries," *IEEE Transaction on Energy Conversion*, vol. 7, no. 1, p. 6, 1992.

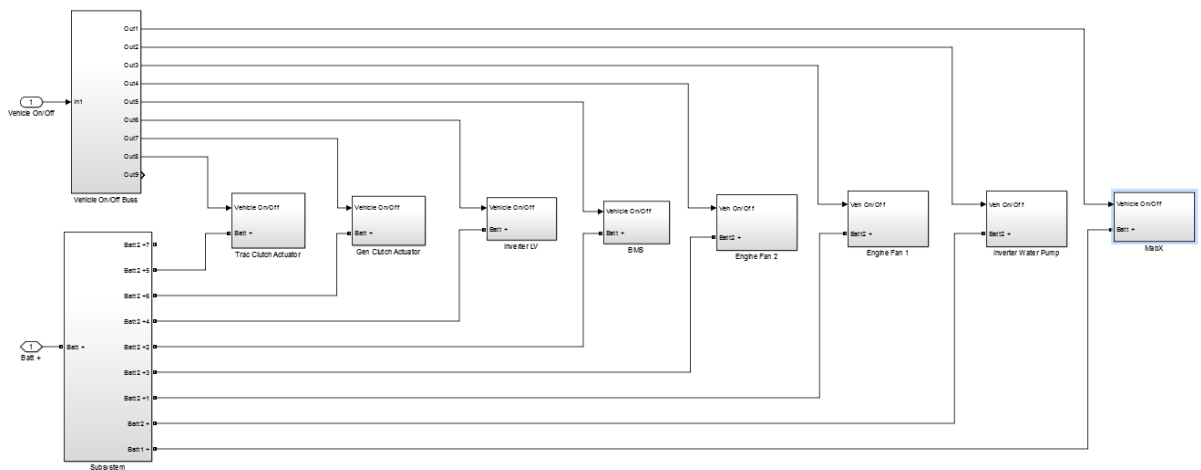
- [16] K. Morison, H. Hamadani and L. Wang, "Practical Issues in Load Modeling for Voltage Stability Studies," *IEEE*, p. 6, 2003.
- [17] N. Guder, "Dynamic Vehicle Electrical System Simulation," *Porsche Engineering Magazine*, p. 3, 2015.
- [18] D. Lambert, "Lead Acid Battery Lifecycle: Terms and Definitions," *Data Center Science Center*, p. 6, 2016.
- [19] C. C. Hua and M. Y. Lin, "A study of Charging Control of Lead-Acid Battery for Electric Vehicles," in *Industrial Electronics*, Cholula, Puebla, 2000.
- [20] T. Morgan, "Guide to Charging Sealed Lead Acid Batteries," Silvertel, Newport.
- [21] POWERTHRU, "Lead Acid Batteries working - LIFETIME STUDY".
- [22] M. Wens and M. Steyaert, "Basic DC-DC Converter Theory," in *Design and Implementation of Fully Integrated Inductive DC-DC Converters in Standard CMOS*, Columbus, Springer, 2011, p. 38.
- [23] R. W. Erickson, "DC-DC Power Converter," *Electrical and Electronics Engineering*, p. 19, 15 June 2007.
- [24] A. S. Limjoco, "Measuring Output Ripple and Switching Transient in Switching Regulators," *Analog Devices*, p. 8, 2013.
- [25] Ericsson Power Modules, "Output Ripple and Noise Measurement Methods for Ericsson Power Modules," *Design Note*, p. 6, July 2010.
- [26] Emerson Network Power, "Effects of AC Ripple Current on VRLA Battery Life," Columbus, 2009.
- [27] C & D Technologies, "Charger Output AC Ripple Voltage and the affect on VRLA batteries," Blue Bell, 2012.

Chapter 7 Appendix

7.1 Appendix A

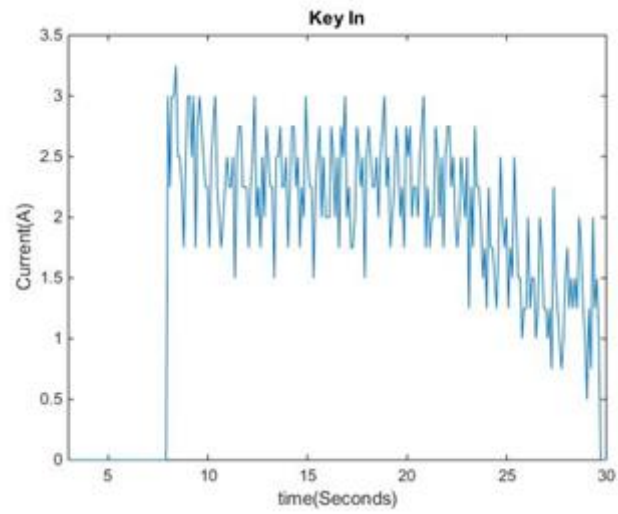


A 1: HV Inverter with Motor Model

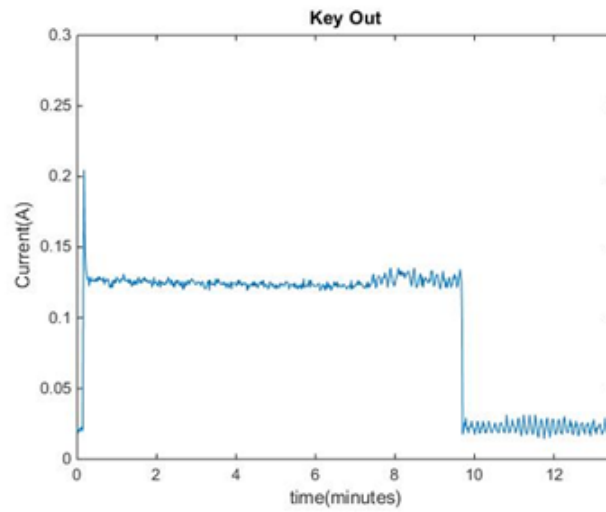


A 2: Overall added components model

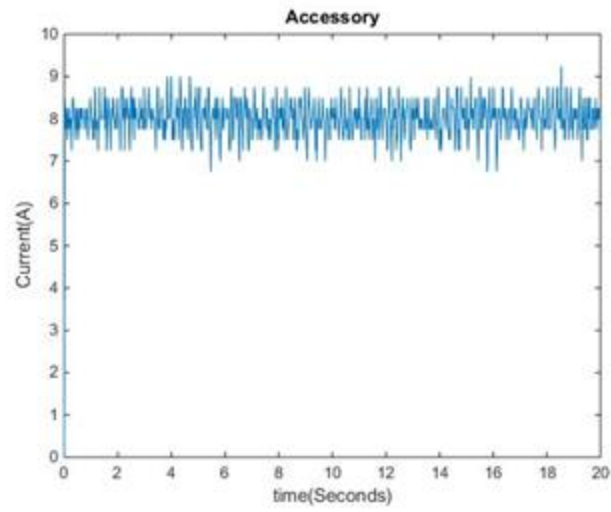
7.1 Appendix B



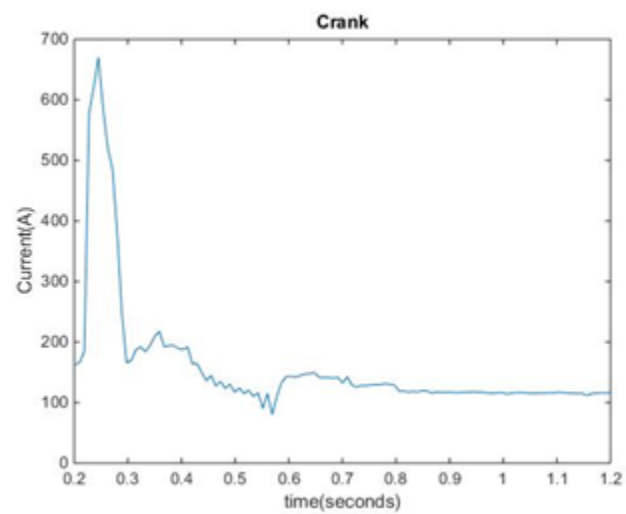
B 1: Stock Key in Current



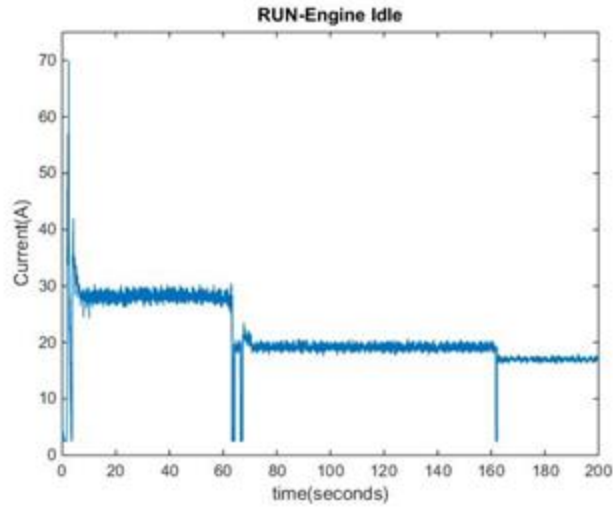
B 2: Stock Key out Current (amps)



B 3: Stock Accessory Loads Current (amps)



B 4: Stock Crank Current (Amps)



B 5: Stock Engine Idle Current (Amps) Data

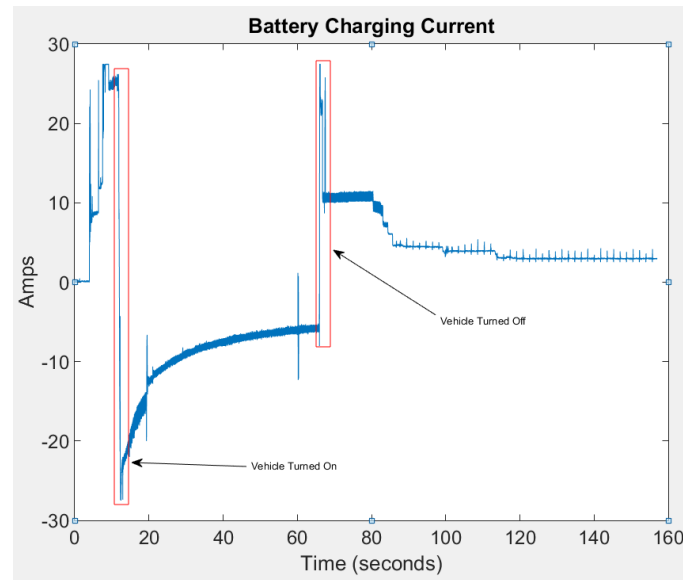
7.1 Appendix C

Subsystem/Component	Loads	Values
Accessory Loads	RLC 1	$1.5\Omega, 10^{-3}\text{H}, 0\text{F}$
	RLC 2	$90\Omega, 10^{-3}\text{H}, 10^{-12}\text{F}$
	RLC 3	$100\Omega, 10^{-3}\text{H}, 0\text{F}$
	RLC 4	$1.2\Omega, 10^{-2}\text{H}, 0\text{F}$
	RLC 5	$0.2\Omega, 10^{-3}\text{H}, 0\text{F}$
Stock Loads	Ignition	$10\Omega, 0\text{H}, 0\text{F}$
	RLC 1	$0.35\Omega, 0\text{H}, 0\text{F}$
	RLC 2	$0.3\Omega, 0\text{H}, 0\text{F}$
	RLC 3	$0.04\Omega, 0\text{H}, 0\text{F}$
	RLC 4	$1.05\Omega, 10^{-3}\text{H}, 10^{-4}\text{F}$
	RLC 5	$0.3\Omega, 10^{-6}\text{H}, 10^{-3}\text{F}$
Traction Clutch	RLC 0	$8\Omega, 0\text{H}, 10^{-5}\text{F}$
	RLC 1	$10\Omega, 10^{-8}\text{H}, 0\text{F}$
	RLC 2	$8\Omega, 0\text{H}, 0\text{F}$
	Active Power	35W
Traction Clutch	RLC 0	$8\Omega, 0\text{H}, 10^{-5}\text{F}$
	RLC 1	$10\Omega, 10^{-8}\text{H}, 0\text{F}$
	RLC 2	$8\Omega, 0\text{H}, 0\text{F}$
	Active Power	35W
Inverter	RLC	$40\Omega, 0\text{H}, 10^{-6}\text{F}$
	RLC 1	$200\Omega, 10^{-8}\text{H}, 0\text{F}$
	RLC 2	$60\Omega, 0\text{H}, 0\text{F}$

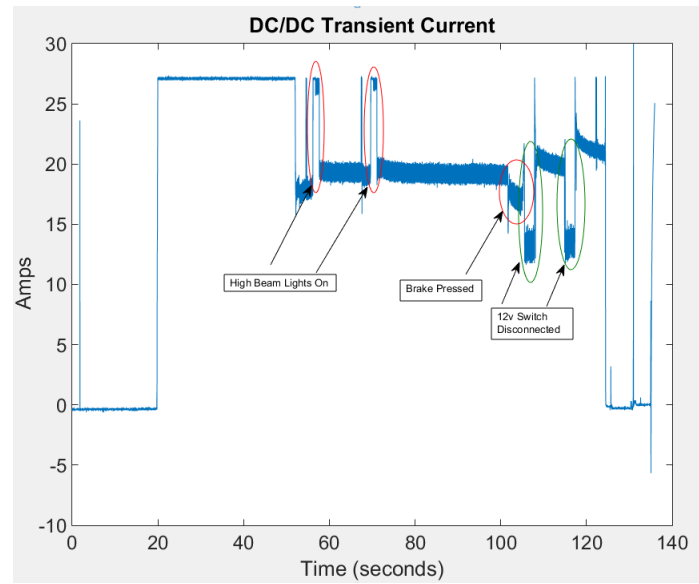
BMS	RLC	$1\ \Omega, 0H, 10^{-5}F$
	RLC 1	$10\ \Omega, 10^{-8}H, 0F$
	RLC 2	$10\ \Omega, 0H, 0F$
Radiator Fan 1	RLC	$1\ \Omega, 0H, 10^{-4}F$
	RLC 1	$3\ \Omega, 10^{-2}H, 0F$
	RLC 2	$4\ \Omega, 0H, 0F$
Radiator Fan 2	RLC	$1\ \Omega, 0H, 10^{-4}F$
	RLC 1	$3\ \Omega, 10^{-2}H, 0F$
	RLC 2	$4\ \Omega, 0H, 0F$
HV system water pump	RLC	$1\ \Omega, 0H, 10^{-4}F$
	RLC 1	$3\ \Omega, 1H, 0F$
	RLC 2	$3\ \Omega, 0H, 0F$
MicroAutoBox	RLC	$1\ \Omega, 0H, 10^{-7}F$
	RLC 1	$11.2\ \Omega, 10^{-8}H, 0F$
	RLC 2	$20\ \Omega, 0H, 0F$

Table 2: RLC Simulation Values

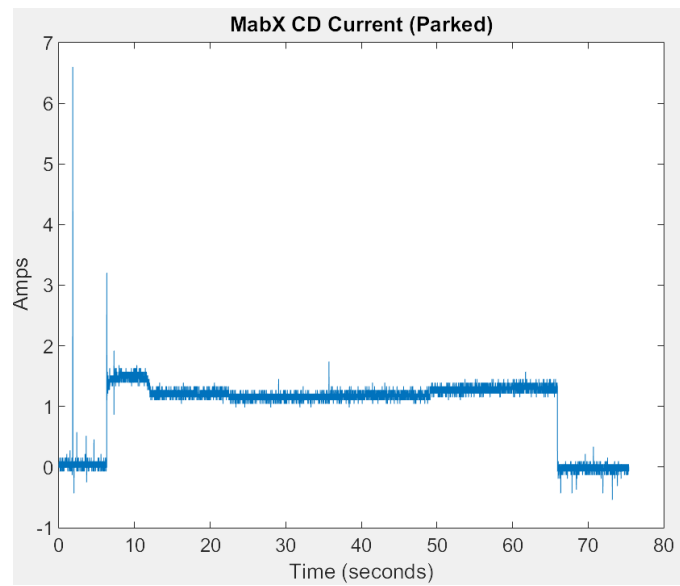
7.1 Appendix D



D 1: More Battery Charging Current



D 2: DC-DC Transient/Initial Turn on



D 3: More Supervisory Current Draw Data with engine on



D 4: Too many ground at one post



D 5: Grounds removed



D 6: Verified Parasitic Current Draw from 12v battery

7.1 Appendix E



AUTOMOTIVE CURRENT TRANSDUCER DHAB S/18



Introduction

The DHAB family is best suited for DC, AC, or pulsed currents measurement in high power and low voltage automotive applications. Its contains galvanic isolation between the primary circuit (high power) and the secondary circuit (electronic circuit).

The DHAB family gives you a choice of having different current measuring ranges in the same housing (from ± 20 up to ± 600 A).

Features

- Open Loop transducer using the Hall effect sensor
- Low voltage application
- Unipolar + 5 V DC power supply
- Primary current measuring range up to ± 30 A for range 1 and ± 350 A for range 2
- Maximum rms primary admissible limited by the busbar, the magnetic core or the ASIC temperature $T^* < +150^{\circ}\text{C}$
- Operating temperature range: $-40^{\circ}\text{C} < T^* < +125^{\circ}\text{C}$
- Output voltage: fully ratiometric (in sensitivity and offset) 2 measuring ranges to have a better accuracy.

Advantages

- Good accuracy for high and low current range
- Good linearity
- Low thermal offset drift
- Low thermal sensitivity drift
- Hermetic package.

Automotive applications

- Battery Pack Monitoring
- Hybrid Vehicles
- EV and Utility Vehicles.

Principle of DHAB Family

The open loop transducers use an Hall effect integrated circuit.

The magnetic flux density B , contributing to the rise of the Hall voltage, is generated by the primary current I_p to be measured.

The current to be measured I_p is supplied by a current source i.e. battery or generator (Fig. 1).

Within the linear region of the hysteresis cycle, B is proportional to:

$$B(I_p) = \text{constant}(a) \times I_p$$

The Hall voltage is thus expressed by:

$$V_H = (R_H/d) \times l \times \text{constant}(a) \times I_p$$

Except for I_p , all terms of this equation are constant. Therefore:

$$V_H = \text{constant}(b) \times I_p$$

The measurement signal V_H amplified to supply the user output voltage or current.

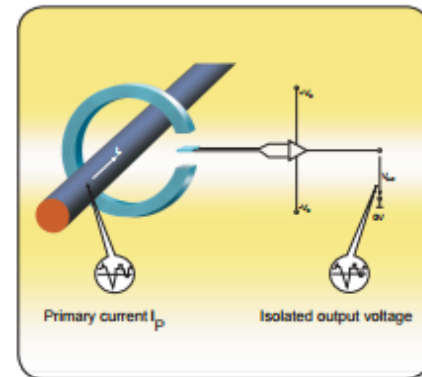


Fig. 1: Principle of the open loop transducer

E 1: Hall Effect Current Sensor used for measuring currents greater than 2 amps

See notes below the data table for battery strings.

[illegible]

Modeling and simulation

- [illegible]

For 50 cells systems that are composed of two 150 mV cell batteries connected in series that are charged with 74 cell chargers to 80% as a useful battery capacity.

- 1) All charging voltage double (due to series connection) as listed in the above table.
- 2) All charging current remain identical to 12 volt numbers as listed above (due to the series connection).
- 3) All charging time remain identical to 12 volt numbers as listed above (due to the series connection).

For 48 volt systems that are comprised of four 12 volt batteries connected in series that are charged with 48 volt chargers with no parallel battery connection.

E 2: Lead Acid Battery Discharge Standards and Calculations